Shallow depth, substantial change: fluid-metasomatism causes major compositional modifications of subducted volcanics (Mariana forearc)

Elmar Albers[1*], John W. Shervais[2], Christian T. Hansen[1], Yuji Ichiyama[3], Patricia Fryer[4]

[1]*MARUM – Center for Marine Environmental Sciences, University of Bremen, Bremen, Germany*

[2]*Department of Geology, Utah State University, Logan, UT, USA*

[3]*Graduate School of Science, Chiba University, Chiba, Japan*

[4]*School of Ocean and Earth Science and Technology, University of Hawaii at Manoa, Honolulu, HI, USA*

* correspondence: Elmar Albers, e.albers@uni-bremen.de

Abstract

Mass transfer at shallow subduction levels and its ramifications for deeper processes remain incompletely constrained. New insights are provided by ocean island basalt (OIB) clasts from the Mariana forearc that experienced subduction to up to ~25–30 km depth and up to blueschist-facies metamorphism; thereafter, the clasts were recycled to the forearc seafloor via serpentinite mud volcanism. We demonstrate that the rocks were, in addition, strongly metasomatized: they exhibit K_2O contents (median = 4.6 wt.%) and loss on ignition (median = 5.3 wt%, as a proxy for H_2O) much higher than OIB situated on the Pacific Plate, implying that these were added during subduction. This interpretation is consistent with abundant phengite in the samples. Mass balance calculations further reveal variable gains in SiO_2 for all samples, and MgO and Na_2O increases at one but the loss of MgO and Fe_2O_3* at the other study site. Elevated Cs and Rb concentrations suggest an uptake whereas low Ba and Sr contents indicate the removal of trace elements throughout all clasts.

The metasomatism was likely induced by the OIBs' interaction with K-rich fluids in the subduction channel. Our thermodynamic models imply that such fluids are released from subducted sediments and altered igneous crust at 5 kbar and even below 200°C. Equilibrium assemblage diagrams show that the stability field of phengite significantly increases with the metasomatism and that, relative to not-metasomatized OIB, up to four times as much phengite may form in the metasomatized rocks. Phengite in turn is considered as an important carrier for K_2O, H_2O, and fluid-mobile elements to sub-arc depths.

These findings demonstrate that mass transfer from subducting lithosphere starts at low *P*/*T* conditions. The liberation of solute-rich fluids can evoke far-reaching compositional and mineralogical changes in rocks that interact with these fluids. Processes at shallow depths (<30 km) thereby contribute to controlling *which components* as well as *in which state* (i.e., bound in which minerals) these components ultimately reach greater depths where they may or may not contribute to arc magmatism. For a holistic understanding of deep geochemical cycling, metasomatism and rock transformation need to be acknowledged from shallow depths on.

1 Introduction

Geologic processes in subduction zones are among the main controllers of chemical cycling (e.g., Stern, 2002, and references therein) that had and still have severe implications for the geochemical evolution and differentiation of Earth. Most importantly, such processes include the liberation of fluids from the subducting slab at ~70–120 km depths that then migrate into the overriding plate where they provoke hydrous partial melting of the mantle. This in turn results in magmatism and tholeiitic to calc-alkaline volcanism and, over long periods of time, the formation of island arcs and continental crust (e.g., Ringwood, 1969; Peacock, 1990; Taylor & McLennan, 1995).

In greater detail, it is the breakdown of hydrous minerals contained in subducting sediments and hydrothermally altered igneous crust and mantle that causes the release of H_2O during prograde subduction metamorphism (e.g., Poli & Schmidt, 1995). Together with the fluids, elements are mobilized and transported into the subduction channel (i.e., the zone at the slab–wedge interface containing the subduction mélange) and the mantle wedge by H_2O, which acts as a primary transport agent for mass in subduction systems (e.g., Bebout et al., 1999; Scambelluri & Philippot, 2001; Ulmer, 2001). Consequently, arc eruptives commonly exhibit a trace element signal indicative of sources that include metasomatized slab-derived components (e.g., Manning, 2004; Rustioni et al., 2021). Eruptives are for instance typically enriched in the incompatible elements B, K, Sr, Cs, Ba, U, and Pb that are traditionally interpreted to originate from sediments and altered oceanic basement and are known as the ‘slab signature’ (Perfit et al., 1980; Tatsumi & Eggins, 1995; Codillo et al., 2018). Arc eruptives provide an important window into deep subduction zone processes and elemental cycling, which have been in the focus of petrologic/geochemical, experimental, and modeling studies over several decades.

Much dehydration of the subducted lithologies, however, occurs long before they reach sub-arc depths. Subducting altered and hydrated basalts, for instance, may contain up to 5 wt.% H_2O—the bulk of which is released during the breakdown of hydrous phases as subduction metamorphism causes the transformation to blueschist (~3 wt.% H_2O) and amphibolite (~1–2 wt.% H_2O) facies assemblages (Poli & Schmidt, 1995). H_2O release from underthrust sediments, due to the compaction and release of interstitial pore waters and mineral dehydration, start as soon as they are subducted (e.g., Moore & Vrolijk, 1992; Bekins et al., 1994). This liberation of fluids at shallow depths is likewise accompanied by significant mass transfer. Slab-derived fluids from several subduction zones have been shown to carry high loads of solutes, in particular elements that are “fluid-mobile” (e.g., at the Nankai Trough or Costa Rica; see review by Kastner et al., 2014).

Whereas slab-derived fluids could be studied at several active convergent margins, most rocks that experienced (and recorded) interactions with such fluids at low- to intermediate-depth subduction conditions originate from paleo-subduction settings. Based on these rocks, now exposed on land, a number of studies advocate minimal fluid and element mobility at low metamorphic grades (e.g., Busigny et al., 2003; Ghatak et al., 2012; see also review by G.E. Bebout in Harlov & Austrheim, 2013). The only active system that provides direct insight into depths up to blueschist-facies conditions is the Mariana convergent margin. Here, recent ocean research drilling efforts (Fryer et al., 2018) have recovered rocks that differ in composition from what has initially been subducted. In this communication we demonstrate that these rock samples are strongly metasomatized and that the changes in composition can well be explained by their interaction with slab-derived fluids (e.g., Mottl et al., 2004). Our study highlights that the metasomatism can to a large degree affect mineralogical assemblages of the lithologies involved, which in turn will affect deeper processes such as the composition of arc magmas and geochemical cycling.

1.1 Serpentinite mud volcanism at the Mariana forearc

The Mariana Trench in the northwestern Pacific marks the subduction of the >180 My old Pacific Plate beneath the Mariana forearc. Together with altered igneous crust, a ~460 m thick sedimentary cover composed of siliceous ooze, volcaniclastic deposits, and pelagic clays is being subducted (Plank et al., 2000; Leat & Larter, 2003). Compaction and early, low-T mineral dehydration result in the release of fluids from the incoming lithologies right after their subduction; these fluids, in turn, hydrate and serpentinize the overlying Mariana forearc mantle wedge (e.g., review by Fryer, 2012). The serpentinite is partly comminuted by tectonic movements and shearing processes at the slab–wedge interface, and deep faults within the forearc crust and mantle facilitate the buoyancy-driven rise of the serpentinite and slab-derived fluids to the forearc seafloor where these erupt in episodic mudflows. Over millions of years, the mudflows have built vast mud volcanoes up to ~50 km in diameter and ~2 km high (Fryer et al., 1985; Fryer et al., 1992). More than a dozen of such serpentinite mud volcanoes are distributed over the forearc seafloor. They formed at varying distances west of the Mariana Trench, tapping the subduction channel at subduction depths of ~13–30 km and temperatures (T) of <80–350°C (Fig. 1; e.g., Fryer et al., 1992;

Oakley et al., 2008; Hulme et al., 2010). The serpentinite mud volcanism provides unparalleled insight into the shallow levels of an active subduction zone.

Five serpentinite mud volcanoes were sampled during three scientific ocean drilling campaigns: Yinazao (55 km distance to the Mariana Trench, ~13 km depth to the slab, ~80°C at the slab–mantle wedge interface), Fantangisña (62 km to trench, ~14 km to slab, ~150°C), and Asùt Tesoru (72 km to trench, ~18 km to slab, ~250°C) during International Ocean Discovery Program (IODP) Expedition 366 (Fryer et al., 2018), and South Chamorro and Conical (78 and 86 km to trench, 18 and 19 km to slab, respectively, with T = 250–350°C at the slab) during previous Ocean Drilling Program (ODP) legs (e.g., Fryer et al., 1992).

Beside serpentinite mud, recovered drill cores contain up to meter-sized boulders of the serpentinized mantle wedge but also materials that originate from the forearc crust and from the subducting Pacific Plate (see next section).

Similar mud flow deposits have been described worldwide from subaerially exposed forearc regions as old as 3.8 By (e.g., Lockwood, 1972; Fryer et al., 1995; Giaramita et al., 1998; Pons et al., 2011), implying that serpentinite mud volcanism in forearc environments occurred throughout the geologic past but requires specific, considerably deformed non-accretionary convergent margin settings.

1.1.1 Serpentinite mud volcanism recycles subducted volcanics

Rock fragments and clasts with mid-ocean ridge basalt (MORB) and ocean island basalt (OIB) provenances were discovered in cores from the serpentinite mudflows of several mud volcanoes. The materials vary in size from millimeter to meter scale and have been identified as subducted, metamorphosed, and recycled materials from the incoming Pacific Plate. Metamorphic mineral assemblages attest up to blueschist facies peak metamorphic conditions (e.g., Maekawa et al., 1993; Fryer et al., 2006; Ichiyama et al., 2021). Most recently, numerous such metamafic rocks were retrieved from the Yinazao, Fantangisña, and Asùt Tesoru mud volcanoes (Fryer et al., 2018). In addition, similar clasts have previously been sampled from South Chamorro and Conical Seamounts (e.g., Fryer et al., 1992). These materials are, to our knowledge, the only blueschist-facies rocks that have been recovered from any active subduction zone.

Petrographic descriptions and (mineral) geochemical compositions of the recycled OIBs from Fantangisña and Asùt Tesoru have been reported by Albers et al. (2019), Fryer et al. (2018, 2020), Deng et al. (2021), and Ichiyama et al. (2021). In many samples, aphyric to coarse grained igneous textures are preserved; aside from rare relict Ti-rich augite, plagioclase, and traces of olivine, apatite, biotite, and Fe–Ti oxides, the igneous mineral assemblages are largely metamorphosed. The clasts are now composed of low- to high-pressure and low- to moderate-temperature metamorphic minerals. These include Ca pyroxene, Na and Ca–Na amphibole, pumpellyite, and phengite at both seamounts, with prehnite, calcite, and zeolites (analcime, thomsonite, natrolite) exclusively reported from Fantangisña and lawsonite and Na pyroxene from Asùt Tesoru (Albers et al., 2019; Fryer et al., 2020; Ichiyama et al., 2021). Metamorphic vein precipitates that formed in apparent equilibrium with slab-derived fluids include pectolite and prehnite at Fantangisña and lawsonite and phengite at Asùt Tesoru; metamorphic calcite and aragonite occur at both settings (Albers et al., 2019). Na pyroxene mainly ranges in composition from aegirine to jadeite, but some analyses exhibit an increased augite component; amphibole is riebeckitic with ferric Fe/Al ratios of up to ~0.45 indicating a strong glaucophane component; phengite is Si-rich with up to 3.88 Si per formula unit (Albers et al., 2019; Fryer et al., 2020; Deng et al., 2021; Ichiyama et al., 2021). These phase assemblages and compositions led Ichiyama et al. (2021) to suggest peak metamorphic grades of prehnite–pumpellyite facies for the clasts from Fantangisña Seamount and of blueschist facies for those from Asùt Tesoru.

The OIB origin of the clasts is implied by bulk rock Ti/V ratios between 50 and 100 (Fig. 2; Fryer et al., 2020; Deng et al., 2021; note that the Ti–V discrimination diagram was recently revised by Shervais, 2021) and by the presence of titanium augite (e.g., Albers et al., 2019). Geochemically, concentrations of SiO_2, MgO, and Na_2O in the recycled OIBs appear to generally overlap with those of volcanic seamounts situated on the Pacific Plate but Fe_2O_3*, i.e., FeO and Fe_2O_3, and CaO are generally lower whereas K_2O and loss on ignition (LOI) are much higher (Fig. 3 & Tab. 1; Fryer et al., 2018; Deng et al., 2021). These distinct compositions have, however, not been in the focus of the above studies. In this work, we will focus on the (modified) compositions of the recycled OIBs, which we attribute to fluid metasomatism that occurred in the subduction zone, and its implications for mass transfer and geochemical cycling.

2 Methods

2.1 Bulk rock geochemistry

To expand the existing dataset by Fryer et al. (2018) and Deng et al. (2021) we have analyzed four additional OIB samples for their major element bulk compositions. Analyses were carried out with a Panalytical® 2400 sequential X-ray fluorescence spectrometer at Utah State University using methods described in Shervais et al. (2019).

2.2 OIB reference compositions

As reference OIB compositions we downloaded data from the PetDB Database (www.earthchem.org/petdb) on 16-02-2021. We extracted all entries with the label ‘Seamount’ situated in the Pacific Ocean (*n* = 3,216). We then narrowed down the composition representative for alkali basalt/OIB by filtering (i) for Ti/V ratios between 50 and 100 (*n* = 75) following the discrimination method developed by Shervais (1982; note that Shervais, 2021, recently revised the field indicating plume-derived basalts to Ti/V = 43–100); (i) for MgO within 8–16 wt% (*n* = 437) to minimize crystal fractionation and accumulation effects (cf., e.g., Jackson & Dasgupta, 2008); (iii) a combination of the two, i.e., Pacific seamount compositions run through a Ti/V–MgO-filter (*n* = 17); (iv) filtering for seamounts in the northern hemisphere only (*n* = 1703). In addition, we compiled compositions of seamounts located in the northwestern Pacific Ocean, east of the Izu–Bonin–Mariana subduction zone. These include data from the Magellan Seamounts (Koppers et al., 1998; Tang et al., 2019; Liu et al., 2020), the Marshall Seamounts (Davis et al., 1989), and from drill core recovery from Deep Sea Drilling Project Site 61, west of the Magellan Seamounts (Janney & Castillo, 1999), and ODP Sites 865 and 866, the Allison Guyot and Resolution Guyot at the Mid-Pacific Mountains (Baker et al., 1995). This latter compilation has 91 entries, of which we excluded the upper and lower 5% to account for outliers. The median reference compositions are presented in Tab. 2.

2.3 Theriak/Domino thermodynamic modeling

Equilibrium assemblage diagrams, commonly termed pseudosections, and mineral abundances were calculated using the Theriak/Domino software package, Version 15-03-2018 (de Capitani & Brown, 1987; de Capitani & Petrakakis, 2010). Calculations are based on the internally consistent thermodynamic database tcds62 from Holland & Powell (2011), but we suppressed the formation of microcline, julgoldite (FeFe), and iron as they were not observed in the recycled OIBs. The database comes with solid solutions for olivine, ortho- and clinopyroxene, spinel, feldspar, biotite, epidote, phengite, chlorite, and chloritoid (Baldwin et al., 2005; Holland & Powell, 1998; Holland & Powell, 2003; White et al., 2007; White et al., 2014a; White et al., 2014b). It does not contain thermodynamic data for K-containing amphibole, which should theoretically result in an overemphasis of K-bearing white mica; however, K_2O contents in amphibole in the metamafics recovered from the serpentinite mud volcanoes are negligible (e.g., Tab. 1 in Fryer et al., 2006; SI in Ichiyama et al., 2021) so that we assume that, if at all, the overemphasis of mica is minor.

Our computations account for the oxide components SiO_2, Al_2O_3, FeO, MgO, CaO, Na_2O, K_2O, and H_2O. Equilibrium assemblage diagrams were compiled for pressure (*P*) = 1–10 kbar, corresponding to up to ~35 km depths when assuming an average lithospheric density of $3*10^3$ kg/m^3, and *T* = 100–600°C; this *P*/*T* range covers the conditions of the slab beneath the Mariana serpentinite mud volcanoes but also the conditions in “warm” subduction zones (Peacock & Wang, 1999). Mineral abundances were calculated for a geotherm of 8°C/km as the equilibrium assemblage of this geotherm best overlaps with the observed mineralogy in the recycled OIBs. Diagrams were compiled for (i) the median composition of NW Pacific seamounts (Tab. 2), which was recalculated to Si 49.51, Al 20.09, Fe 4.67, Mg 10.27, Ca 10.44, Na 5.90, K 1.57, and H 22.65 to use as input for Theriak/Domino, and (ii) the median composition of the recycled OIB clasts (Tab. 1), recalculated to Si 47.60, Al 16.92, Fe 3.47, Mg 9.65, Ca 8.03, Na 4.77, K 5.79, and H 35.02. Additional O was added in both cases to account for the presence of Fe_2O_3 in the hydrothermally altered rocks.

3 Results

3.1 Mass balance constraints on compositional changes

The major elemental compositions of the recycled OIBs reveal K_2O contents (mostly between 3.7–5.5 wt%) and LOI (4.0–7.7 wt%) as a proxy of H_2O much higher than OIB from the Pacific Ocean (Fig. 3; see also Fig. S1 for anhydrous compositions). By contrast, Fe_2O_3 and CaO in the recycled OIBs appear generally lower. Patterns in Al_2O_3, MgO, and Na_2O are inconsistent: clasts from Fantangisña appear to have less Al_2O_3, more MgO, and similar Na_2O relative to Pacific OIB whereas clasts from Asùt Tesoru have similar or higher Al_2O_3 contents but less MgO and Na_2O.

To assess the approximate changes in major element contents of the recycled OIBs, we compared them with basaltic seamounts from the northwestern Pacific (Tab. 2), i.e., hydrothermally altered OIB prior to subduction at the Izu–Bonin–Mariana subduction system (referred to as ‘unsubducted OIB’ from here on). It can be expected that the recycled OIBs were compositionally similar to these unsubducted OIB prior to subduction. Results of our isocon analysis (Gresens, 1967; Grant, 1986) are shown in Figure 4; calculations were done on an anhydrous basis. The results imply the addition of K_2O and variable amounts of SiO_2 to clasts from both seamounts and of MgO to OIBs from Fantangisña when constant mass is assumed. The assumption of constant mass appears reasonable for Asùt Tesoru where TiO_2 and Al_2O_3, both considered rather immobile, lie on the isocon line. At Fantangisña, however, this assumption would suggest the loss of all immobile species—which is unlikely. We hence calculated additional isocon lines assuming the conservation of Al_2O_3 (Fig. 4; Tab. 3). The median slope of these isocon lines at Asùt Tesoru ($y = 1.006x$) is almost identical to the one assuming constant mass ($y = x$). It is, however, much less steep at Fantangisña ($y = 0.747x$); but since the immobile TiO_2 plots well on the conserved-Al_2O_3-line we argue that this assumption is reasonable here. It hence appears (i) that a net increase in mass affected the clasts from Fantangisña but not from Asùt Tesoru and (ii) that the recycled OIBs from Fantangisña gained K_2O, SiO_2, MgO, and Na_2O whereas those from Asùt Tesoru gained K_2O and some SiO_2 but lost Fe_2O_3 and possibly MgO. The bulk of these compositional changes can likely be ascribed to metasomatic processes that accompanied fluid–rock interactions within the subduction system (see discussion).

3.2 Equilibrium assemblage diagrams

Equilibrium assemblage diagrams compiled for the median compositions of unsubducted OIB and the recycled OIBs, respectively, illustrate which phases are to be expected in these rocks. The section for the unsubducted OIB thereby serves as a reference to determine the mineralogical consequences induced by the compositional changes that we ascribe to fluid-metasomatism.

For the unsubducted OIB, quartz, feldspar, pyroxene, epidote, and chlorite are predicted to be stable throughout most of the modeled P/T conditions (Fig. 5a). Prehnite may form below ~3 kbar/200°C. At higher T, biotite and tremolitic amphibole become part of the mineral assemblage. Pumpellyite exists at low T and up to ~10 kbar, together with riebeckite and lawsonite at $P > {\sim}3$ kbar. Glaucophane joins the assemblage at ~4.5 kbar/100°C, persisting between ~200–300°C to higher P. Phengite is restricted to $T < 350$°C. As opposed to this, the equilibrium assemblage predicted for the recycled OIBs strongly differs from the above (Fig. 5b). Quartz is absent except for very low-P/high-T conditions, tremolite is not predicted at all, and no epidote will form at $T < 200$°C. Biotite is present throughout the model conditions, except for intermediate P and $T < {\sim}200$°C. Prehnite exists up to ~4 kbar/350°C, vesuvianite may form at T up to 450°C, and the stability field of pumpellyite is restricted. Riebeckite and glaucophane form at >2 kbar/low T, and lawsonite at high P/low T. Phengite is stable throughout most of the modeled P/T range.

In unsubducted OIB, the equilibrium assemblage along the 8°C/km geotherm is dominated by feldspar, quartz, and epidote until ~6 kbar/150°C, accompanied by minor chlorite and pumpellyite (Fig. 6a). Lawsonite and amphibole contents increase at $T > 150$°C and at 170–200°C the amount of pumpellyite decreases whereas that of pyroxene increases. Amphibole is tremolitic to riebeckitic below ~6 kbar/150°C, and mainly glaucophane at higher P/T conditions (Fig. S3a). Above about 7 kbar/200°C, the mineral assemblage consists of epidote, amphibole, quartz, lawsonite, and pyroxene (mainly diopside in composition; Fig. S3a). About 1.5 mol of phengite exists throughout the prograde path. Contrastingly, with 5–6 mol phengite and >3–4 mol pyroxene present along the 8°C/km geotherm, these two phases dominate the mineral assemblage in the recycled OIBs (Fig. 6b); above 200°C, pyroxene contents even increase to ~9 mol. Diopside and aegirine components in pyroxene are predicted below 200°C, and jadeite pyroxene joins this assemblage at higher P/T conditions (Fig. S3b). Lawsonite is stable even at 3.5 kbar/100°C but is most abundant at $T > 200$°C. Minor amounts of riebeckitic amphibole are formed at $T < 200$°C and moderate to minor amounts of glaucophane at $T > 150$°C (Fig. S3b). Chlorite and feldspar exist up until 6 kbar/160°C, and the presence of pumpellyite is restricted to ~160°C at 6 kbar and 220°C at 8 kbar.

4 Discussion

4.1 Transfer of mass within the Mariana forearc

4.1.1 Subduction metasomatism vs. seafloor alteration processes

It has long been known that subduction zones are sites of major mass transfer and chemical cycling. The meta-OIB data reported by Fryer et al. (2018), Deng et al. (2021), and in this study provide direct evidence for mass transfer at shallow levels of the Mariana convergent margin. Most striking are increases in K_2O and LOI, but our mass balance calculations imply that SiO_2, MgO, and Na_2O are also modified (Fig. 4; Tab. 3).

In general, subducting lithologies undergo prograde metamorphic phase changes in response to rising P and T with increasing depth. Such transformations could (theoretically) occur in geochemically closed systems, in which the phase assemblages of the subducting lithologies would change, but the bulk rock would retain its composition. Contrastingly, fluid-induced metasomatism can lead to the transfer of mass into or away from individual pieces of rock, modifying their bulk composition. Absolute increases in certain elements should hence be mainly the result of the interaction with fluids that transported the respective elements; losses in element concentrations are usually ascribed to the breakdown of out-of-their-stability-field minerals and the fluid-mediated removal of the released elements (e.g., Putnis & Austrheim, 2010).

Quantitatively assessing the compositional changes of the recycled OIBs remains difficult because their exact compositions prior to subduction are unknown. It can be assumed that they were generally similar to OIB situated in the northwestern Pacific Ocean—but the compositions of such vary to a certain degree as analyzed sample suites usually cover a range of primary and secondary processes (such as magmatic differentiation and crystal accumulation effects or hydrothermal alteration, respectively; cf. Fig. 3; see also Figs. S2). The problem of attributing compositional changes to fluid–rock interactions within the subduction zone becomes particularly clear when considering, for instance, MgO contents in the recycled OIBs of which most overlap with that of the unsubducted OIB (Figs. 3 & S1). The relatively higher values at Fantangisña (median = 10.3 wt% *vs.* 4.5 wt% at Asùt Tesoru) could potentially be explained by the aforementioned primary or secondary processes. Indeed, when compared to the MgO–Ti/V-filtered data of all Pacific seamounts, some samples contain up to ~12 wt% MgO (gray diamonds in Fig. 3). By contrast, K_2O contents of the recycled OIBs (median = 4.5 wt% at Fantangisña and 4.7 wt% at Asùt Tesoru) clearly exceed those of unsubducted seamounts (up to 4 wt%; median = 1.15 wt%), so it appears improbable that these enrichments have been induced prior to subduction. Similarly, we argue that SiO_2 (median = 48.2 wt% in the recycled OIBs; median = 50.9 wt% on an anhydrous basis) has been added to most clasts during subduction: hydrothermal alteration of basalts at the seafloor admittedly also increases SiO_2 (e.g., Staudigel et al., 1996) and similar contents in unsubducted OIB are not uncommon (50% of data between 44.6–47.2 wt.%; Figs. 3 & S1), but the observed gains in K_2O and H_2O would dilute these values to <<46 wt%. Our isocon analysis further imply that Na_2O was gained in the OIBs from Fantangisña whereas Fe_2O_3* was lost from those from Asùt Tesoru (Fig. 4).

Altogether, it cannot be excluded that some of the differences between unsubducted and recycled OIBs represent a sampling bias and/or seafloor alteration processes. But in particular the increases in K_2O and H_2O, as well as, to a lesser extent, SiO_2 and Na_2O can presumably be attributed to fluid-metasomatism during subduction. This transfer of mass can be well explained by the presence of solute-laden fluids in the Mariana forearc that are particularly abundant and well documented (e.g., Mottl et al., 2004; Savov et al., 2007; see below). The lateral distance of >160 km between the Fantangisña and Asùt Tesoru Seamounts, together with the fact that K_2O–SiO_2-enriched OIBs were recycled at both sites, suggests that the metasomatic processes are not a local phenomenon but are widespread in the Mariana Subduction System.

4.1.2 Fluid processes and OIB alteration

Fluid and solute release following mineral breakdown reactions in the subducting slab can be traced at the outer Mariana forearc by slab-derived fluids that expel at the serpentinite mud volcano summits. The compositions of these slab-derived fluids systematically change across the forearc, in response to prograde metamorphic processes at depths of ~10–30 km and T = <80–350°C (e.g., Mottl et al., 2004; Savov et al., 2007; Hulme et al., 2010; Fryer et al., 2018). The inferred processes in the slab range from sediment compaction and opal-CT dehydration at shallowest levels to clay diagenesis and dehydration, the release of desorbed water, and decarbonation at greater depths (Mottl et al., 2004; Hulme et al., 2010; Menzies et al., 2021). The decarbonation of subducted sediments and AOC (altered igneous portions of the oceanic crust), for instance, is thought to result in high carbonate alkalinity in slab-derived fluids of the deeper-sourced mud volcanoes relative to shallow-sourced ones. High alkalinity in turn favors the precipitation of $CaCO_3$ below the deep-sourced mud volcanoes, leading to a depletion of Ca and Sr in the fluids that rise to the forearc seafloor. By contrast, Ca and Sr in pore waters at the shallower-sourced mud volcanoes are enriched because the slab is still too cold for decarbonation to occur (Mottl et al., 2004). Expressed in numbers, Ca decreases from >50 mmol/kg to <1 mmol/kg and Sr from >500 µmol/kg to <20 µmol/kg (see compilations in Wheat et al., 2018; Menzies et al., 2021). Similarly, K, Rb, Cs, and B are thought to be leached from the subducted sediments and AOC once the slab has warmed to T > 100–150°C (Mottl et al., 2004; Hulme et al., 2010). Concentrations of these in the serpentinite mud pore waters as a result increase from shallow- to deep-sourced sites across the forearc. Concentrations of K change from <1 mmol/kg to >15 mmol/kg, Rb increases from <1 µmol/kg to >5 µmol/kg, Cs from <5 nmol/kg to >>50 nmol/kg, and B from <1 µmol/kg to >3,000 µmol/kg (Wheat et al., 2018). Contents of Si are generally low in the serpentinite mud pore waters (Geilert et al., 2020) since Si is readily taken up by the forearc mantle peridotite during serpentinization (e.g., Albers et al., 2020; Geilert et al., 2021). But Si contents in slab-fluids were likely much higher shortly after their release, as originating, for instance, from opal diagenesis and/or the transformation of smectite to illite (cf., e.g., Mottl et al., 2004; Kastner et al., 2014).

In the subduction channel, comminuted material as well as rock clasts react with these fluids. Serpentinites, previously entitled "sponges" for fluid-mobile elements (Deschamps et al., 2011), can contain high concentrations of Rb, Cs, B, and other fluid-mobile elements (e.g., Debret et al., 2019; Albers et al., 2020). Contents of K_2O in the serpentinite clasts and mudflows are, however, low with on average <<0.1 wt% (e.g., Savov et al., 2005a; Savov et al., 2005b)—despite the general availability of K at the deeper-sourced mud volcanoes (see above). This is presumably the case because serpentinite phases do not incorporate K in their structure. In consequence, the forearc serpentinite does not act as a sink for K. Following this line of thought, K-rich fluids are likely available to react with any lithology in the subduction channel that could form K-bearing minerals. Such lithologies encompass subducted mafics, including OIB, which provide the components and the chemical environment to form phengite or biotite.

The uptake of K has been mostly pervasive, as evidenced by the abundant replacement of former groundmass by phengite in the recycled OIBs (Fig. 6 in Fryer et al., 2020) and the shortage of K-bearing phases in metamorphic veins (Albers et al., 2019). Indeed, no such phases have been observed in OIBs recycled at Fantangisña. In addition, we generally observed less phengite in the samples from Fantangisña and also little other K-bearing minerals so that it remains somewhat enigmatic which phases account for the strong K_2O increase.

Likewise, the differences in metasomatic element uptake between the clasts from Fantangisña and Asùt Tesoru (Fig. 4) are to some extent questionable and cannot unequivocally be clarified in this study. The recycled OIB clasts from both sites should, theoretically, have experienced similar P/T paths as well as interactions with similar slab-fluids when assuming (i) homogeneous compositions of the incoming altered oceanic crust and (ii) similar exposure times to slab-fluids in the subduction channel. But OIBs from Fantangisña, the shallower-sourced seamount, are marked by a net increase in mass and uptake of K_2O, SiO_2, MgO, and Na_2O and those from Asùt Tesoru, the deeper-sourced site, show increases in K_2O and SiO_2 and possibly losses of MgO and Fe_2O_3*. Given these distinctions, we follow that (i) and/or (ii) must be incorrect. But even when considering variations of the subducting lithosphere at the two sites (being >160 km apart) it is difficult to explain the loss in MgO (and Fe_2O_3*) in the Asùt Tesoru OIBs, since the subduction channel mélange, the mud volcano conduits, and the mudflows in which the clasts resided are overall characterized by ultramafic, Mg–Fe-rich materials. The second possibility would be that the exposure times of the Asùt Tesoru samples within the Mg-rich environment were much shorter as compared to the Fantangisña OIBs, but similar enrichments in K_2O between the two sites suggest otherwise. In contrast, the addition of MgO (and maintenance of Fe_2O_3*) in the samples from Fantangisña appears plausible in this overall ultramafic environment; comparably, MgO contents in seafloor basalt typically increase as a result of hydrothermal alteration and chlorite formation at similar T (e.g., Staudigel et al., 1996; Bach et al., 2013). The gain in SiO_2 in samples from both mud volcanoes was potentially pervasive—we assume that slab-fluids have initially been siliceous (see above)—but may in addition be explained by the presence of silicates in metamorphic veins: pectolite, prehnite, white mica, and lawsonite occur at both study sites (Albers et al., 2019). Pectolite ($NaCa_2Si_3O_8(OH)$), however, appears to be more frequent in OIBs from Fantangisña, which partly explains the Na_2O increase in these samples. Further, plagioclase feldspar in these samples may be Na-rich as is typical for altered seafloor basalts (Alt, 1995). Feldspar is predicted to be stable at rather low *P*/*T* along the 8°C/km isotherm (Fig. 6b), which could indicate that it is part of the equilibrium assemblage in clasts from Fantangisña but not in those from the deeper-sourced Asùt Tesoru. In the latter, the replacement of plagioclase by lawsonite and phengite (see Fig. 6 in Fryer et al., 2020) lends further credence to this idea. During this process, some of the Na from the plagioclase's albite component is possibly being released from the rocks and hence explains the clasts' lower Na_2O contents. After all, aside from heterogeneities in the composition of the subducting crust, it may be this and similar breakdown reactions/changes in mineral stabilities that explain the variations between the OIBs from the two mud volcanoes that tap different *P*/*T* conditions at the subduction channel.

4.1.3 *P*/*T* conditions and ramifications of metasomatism for mineral stabilities

The observed compositional changes have direct implications for the thermodynamic stability of mineral phases. This is most striking for the stability field of phengite that is limited to <300°C in unsubducted OIB but, for the metasomatized ones, is increased to 600°C at both cold and warm subduction zones (Fig. 5). In addition, besides this larger stability field, considerably larger quantities of phengite (about 6 instead of 1.5 mol; Fig. 6) are being predicted for the metasomatized OIBs.

The exact geotherm and the respective *P*/*T* conditions in the Mariana subduction system remain vague. The depths to the slab below the mud volcanoes—from which *P* conditions can be derived—could relatively well be determined using multi-channel seismic reflection data (e.g., Oakley et al., 2008). But estimates on *T* conditions are less precise because they chiefly rely on interpretations of equilibrium mineral assemblages and mineral compositions in metamafic clasts (e.g., Maekawa et al., 1993; Oakley, 2008), on across-forearc changes in pore water compositions of the serpentinite mud (e.g., Mottl et al., 2004; Menzies et al., 2021), and on oxygen stable isotope compositions of serpentine–magnetite pairs. The serpentine–magnetite pairs, for instance, imply serpentinization *T* of up to 400°C for samples from Asùt Tesoru Seamount (Debret et al., 2019), whereas metamafic mineral assemblages and compositions imply *T* of 200–250°C for that seamount (Ichiyama et al., 2021). To make matters worse, the travel paths from depths to the forearc seafloor are not completely understood; several authors have suggested that both metamafic and serpentinite clasts may travel upwards in the subduction channel after having been subducted to greater depths (e.g., Tamblyn et al., 2019) and before being entrained by mud volcanism. They could hence have experienced *P*/*T* metamorphic conditions greater than those below the individual mud volcanoes. In this sense, a blueschist clast from South Chamorro Seamount was interpreted to have experienced up to 19 kbar and 590°C (Tamblyn et al., 2019).

The pressure at the slab is despite these uncertainties estimated at ~4 kbar below Fantangisña (~14 km slab depth) and 6 kbar below Asùt Tesoru (~18 km; Oakley et al., 2008), with T of ~150°C and 250°C, respectively. Resultant geothermal gradients would span a range of 10–14°C/km or even 6–17°C/km when including the P/T estimates for the other serpentinite mud volcanoes (see, e.g., Table 1 in Fryer et al., 2020). Several factors may lead to inaccuracies and explain this large range. For instance, the complex topography of the subducting Pacific Plate implies a high relief of the slab–wedge interface (Fryer et al., 2020). Topographic highs such as subducted seamounts could hence cause seismic reflections and be interpreted as the top of the subducting slab; these may, however, protrude from the surrounding subducting seafloor by several kilometers and hence affect the depth estimates. Temperature estimates on the other hand, in particular the ones based on metamorphic mineral assemblages, may be biased by the time the metamorphism occurred. Shortly after the subduction initiation in the Eocene, the mantle wedge was much hotter than today, which would lead to higher-grade metamorphism at a given depth of the subduction channel than today (Ichiyama et al., 2021). In support of this interpretation, age-dating metamorphic minerals in blueschist clasts from South Chamorro Seamount revealed formation ages of >45 Ma (Tamblyn et al., 2019).

The geotherm of ~8°C/km appears to be best consistent when comparing the observed mineral assemblages (Albers et al., 2019; Fryer et al., 2020; Deng et al., 2021; Ichiyama et al., 2021) with our equilibrium assemblage diagrams (*cf.* Fig. 5b). Following this isotherm, jadeitic pyroxene only joins the metamorphic assemblage at ~7 kbar/200°C (Fig. S3b), which would be the absolute minimum P/T conditions the clasts at Asùt Tesoru Seamount have experienced. The key criterion for such a geotherm is the presence of lawsonite, which is not predicted for steeper geotherms, e.g., of 10°C/km (dashed line in Fig. 5b). Following this argument, the lack of lawsonite in OIBs from Fantangisña Seamount implies $P \leq 4$ kbar—which would further implicate ~100°C when following the 8°C/km geotherm. The T the OIBs experienced was, however, likely higher as implied by the presence of pumpellyite that is restricted to 160–220°C. It must yet be kept in mind that the computed phase diagram applies to the recycled OIB's median composition. Due to compositional differences between individual clasts and between Fantangisña and Asùt Tesoru, (minor) deviations between the predicted and the observed mineral assemblages and their compositions are not unlikely. For instance, amphibole is predicted to be mainly glaucophane above ~5.5 kbar/150°C, with a limited riebeckite component; lower MgO in the clasts from Asùt Tesoru relative to those from Fantangisña (Fig. 3) would potentially decrease the glaucophane fraction in amphibole. Allowing, during thermodynamic modeling, only for the formation of amphibole with compositions similar to those observed by Ichiyama et al. (2021), i.e., $\mathrm{Rbk_{0.65}Gln_{0.35}}$, results in a very similar mineral assemblage (Fig. S4). The amount of amphibole, however, is lower in particular at intermediate P/T at which instead higher amounts of pyroxene are predicted, and pumpellyite is stable up to somewhat higher *P*/*T* conditions. The predicted pyroxene compositions (similar amounts of the aegirine and jadeite components; Fig. S5) are also similar to those analyzed by Ichiyama et al. (2021). Further, the lower bulk Al_2O_3 in the OIBs recycled at Fantangisña (median = 10.9 wt% vs. 16.0 wt% at Asùt Tesoru; Fig. 3) may explain lower amounts of phengite (Albers et al., 2019; Ichiyama et al., 2021) in clasts from this mud volcano, since Al is an important constituent in the muscovite component of phengite.

Aside from the compositional variability, the metasomatism of the clasts is a continual process: they react with fluids with evolving solute loads (in response to increasing *P*/*T* conditions) while being dragged to greater depths. Some of the metasomatism likely occurred at relatively late stages, i.e., after the subduction to and metamorphism of the (at that time only partly metasomatized) OIB clasts at a certain depth. As metamorphic reactions can be considered generally rather sluggish at the considered *P*/*T* range, the clasts' equilibration with the ever-evolving slab-fluid should lag behind and *P* and *T* overstepping may be needed for the reactions to proceed (e.g., Pattison et al., 2011). This assumption is supported by the presence of vein mineralogies in the metamafics that are distinct from the phase assemblages in the clast's groundmasses. Sodic amphibole, pumpellyite, and chlorite for example replace Na pyroxene or the igneous groundmass (Ichiyama et al., 2021) but have not been observed in veins that formed in apparent equilibrium with the slab-derived fluids in the subduction channel (Albers et al., 2019). Following this line of thought it would be possible that phases such as lawsonite formed in the subducted OIB before the rocks were metasomatized to their current compositions.

Taken together, a reasonable consensus between observations and models exists. However, reproducing the metamorphic phase assemblages by equilibrium modeling is impeded by compositional variabilities, the timing of the metasomatism, and potentially by partial out-of-equilibrium states of the clasts. We estimate the geothermal gradient at 8–10°C/km, whereby the lower gradient appears realistic for today's mature subduction zone in which mantle wedge has been cooled by the >180 My old subducting Pacific Plate since the Eocene. Metamorphism in the geologic past may have occurred at higher *T*. Our model results hence strengthen previous studies suggesting ~4 kbar/up to 160–220°C for the OIBs recycled via the Fantangisña mud volcano and up to 7–8 kbar/200–350°C for those from Asùt Tesoru. The metasomatic changes in bulk composition markedly increase the stability field of phengite.

4.2 Thermodynamic constraints on fluid-metasomatism at intermediate *P*/low–intermediate *T*

We carried out thermodynamic reaction path modeling to better understand the fluid–rock reactions in the subduction channel and the most obvious metasomatic changes, i.e., the transfer of K_2O from the subducting slab into OIB. The models are thought to provide a generalized view of mass transfer at subduction depths of 15–20 km.

Sediments being subducted at the Mariana Trench consist of chert, radiolarite, volcanic turbidites, and pelagic clay, of which only the turbidites and clay contain significant amounts of K_2O (up to ~1.9 wt% and 3.9 wt%, respectively; Plank & Langmuir, 1998). The limited thicknesses of these units east of the Mariana Trench (190–220 m and 40–80 m, respectively; Plank et al., 2000) restrict the overall amounts of K_2O that can be liberated from these. The other main source for K_2O in the slab-derived fluids is subducting AOC. At a global scale, AOC has on average 0.65 wt% K_2O (Staudigel, 2014) but contents in the Cretaceous basalts east of the Mariana Trench can exceed 5 wt% (ODP Site 801; Kelley et al., 2003). The igneous basement is hundreds of meters thick, providing a vast reservoir for K_2O.

As starting compositions in the models, we used bulk sediments east of the Mariana Trench, AOC (the conservative composition with 0.65 wt% K_2O), and a 50:50 mixture of the two. The modeling consists of two steps: (i) to approximate the composition of the fluid that is released from the slab, we equilibrated sediments, AOC, and the 50:50 mixture, respectively, with a fluid at $P = 5$ kbar, varying T (150–400°C in 50°C steps), and a final fluid/rock mass ratio (f/r ratio) of 0.1; (ii) to mimic fluid–rock reactions in the subduction channel, we reacted a median NW Pacific OIB composition with the fluid resulting from (i), at $P = 5$ kbar, $T = 200$ and 300°C, and a final f/r ratio of 10. Details on the models and thermodynamic data are provided in the Supplementary Information.

Modeling results of the AOC–OIB runs are summarized in Figure 7; results from the other setups are presented in Figure S6. In all cases, K as well as Si, Ca, and Na are mobilized from the starting lithologies (Figs. 7a & S6a). Solute concentrations in the fluids are, however, strongly dependent on T and partly dependent on the f/r ratio; concentrations can vary by a factor of ten and more. The corresponding mineral assemblages predicted for the subducted slab are shown in Figure S7. Upon the reaction of the solute-laden fluids with OIB, mineral assemblages are dominated by epidote, phengite, and chlorite at 200°C with abundant lawsonite at fluid-dominated and quartz at more rock-dominated conditions when the fluid is (partly) sourced in subducting sediment (Figs. 7b & S6b). At 300°C, plagioclase, epidote, and phlogopite characterize the equilibrium assemblage in the model runs following AOC and AOC–sediment equilibration, with minor hematite and chlorite as well as minor phengite at high f/r ratios. By contrast, the sediment–OIB models predict dominantly quartz and garnet together with talc and stilpnomelane (at high f/r ratios) and chlorite (towards lower f/r ratios). Bulk K_2O contents in the now metasomatized OIBs have doubled over most of the model conditions at 200°C, now exceeding 2 wt% except for strongly fluid-dominated systems and towards completed reaction in the sediment–OIB runs (Figs. 7c & S6c). At 300°C, K_2O even approaches 3 wt.% in the AOC–OIB models whereas a loss of K_2O from the OIB is predicted for the sediment–OIB models. The major hosts of K_2O are phengite and phlogopite at 200°C and 300°C, respectively.

Our modeled fluid compositions are generally consistent with observations from the serpentinite mud volcanoes in that they imply considerable mobilization of mass from the slab at shallow depths and low *T*. The fluids in the Mariana forearc, however, undergo severe compositional changes during the reaction with solids in the subduction channel and during their rise to the forearc seafloor (e.g., loss of Si and Ca; see Section 4.1.2), so that the modeled fluid compositions cannot directly mirror those recorded in the serpentinite mud pore waters. But, for instance, the presence of abundant prehnite and pectolite with equilibrium growth structures in metamorphic veins in the recycled OIBs (Albers et al., 2019) lends strong credence to the existence of Si–Ca–Na–K-containing fluids. Further, the corresponding phase assemblages in the fluid source lithologies (Fig. S7) appear reasonable for the physicochemical (modeling) conditions: comparable assemblages were described as alteration products in mafic rocks and/or sediments that experienced metamorphism up to blueschist grade overprints (e.g., Ernst, 1984; Jayko et al., 1986). Phases predicted to be stable in the metasomatized OIB (Figs. 7c & S6c) resemble those in metabasaltic rocks that were interpreted to have reacted with slab-derived fluids at shallow subduction levels, such as greenstones and blueschists from the Franciscan Complex (e.g., Bebout & Barton, 1993; Ukar & Cloos, 2014).

It must be kept in mind, however, that our models oversimplify the natural system by assuming complete chemical equilibrium between all reactants, by not including kinetic effects, as well as by the possible shortage of relevant low-*T* mineral phases in the thermodynamic database. The models cannot emulate the vast complexity of natural reactions taking place in subduction zones, which are influenced by factors such as the physicochemical conditions during dehydration (*T* and f/r ratios), heterogeneities in type, composition, and alteration of subducting lithologies. For example, Staudigel et al. (2010) speculated that volcaniclastic sediments, providing the greatest share of K as sedimentary input to the Mariana subduction zone, should be particularly predominant close to large seamounts; following the arguments in Mottl et al. (2004), it is very likely that K will be released from the slab, in particular from volcanic turbidites, presumably even at *T* lower than those in our models. The average composition of subducting sediments used as input in our models will not take account of such variations. In addition, we also did not consider interactions between the different lithologies in the subduction channel, e.g., between ultramafic material and OIB, which would have added further complexity. More dedicated modeling and possibly experimental work would be needed to better reflect those natural fluid–rock interactions.

The key observations are, however, that at shallow subduction conditions (i) the release of K-containing fluids from subducting sediments and from AOC as well as (ii) the uptake of K_2O by OIB, i.e., K_2O-metasomatism, are thermodynamically plausible, and (iii) that this may lead to the formation of substantial amounts of phengite or other K-bearing phases. The models, in addition, imply K and other solutes such as Si, Ca, and Na to be elevated in slab-derived fluids at convergence margins across a range of thermal conditions, i.e., at both cool and warm subduction settings. The results hence strongly support the feasibility of metasomatic changes of (mafic) materials to occur in subduction channels at depths << 30 km.

4.3 Implications of forearc metasomatism and the role of phengite in element cycling

Following the results from this study, and from the research conducted at the Mariana forearc over several decades, it has become clear that incoming lithologies must considerably change their composition at forearc depths. Independent of uncertainties in peak metamorphic conditions, this shallow transfer and redistribution of mass potentially has profound implications for processes at deeper subduction levels. The shallow removal of certain elements from the subducting lithosphere affects the compositions of rocks that are subducted to beyond-forearc depths. Likewise, the mobilized elements impact fluid–rock reactions in the subduction channel and the mantle wedge. Low- to intermediate-grade metamorphic/metasomatic phases formed here, such as lawsonite and phengite (Figs. 5 & 6), will transport H_2O and elements to greater depths. Both minerals have extensive stability fields up to depths of >200 km (e.g., Poli & Schmidt, 1995; Schmidt, 1996). Phengite contains about 4 wt% H_2O and 12 wt% K_2O and is considered as an important carrier for these to and beyond sub-arc depths.

It is hence questionable whether K_2O and H_2O captured in phengite will ultimately be available to contribute to arc magmatism (also see discussion on phengite breakdown in, e.g., Chen et al., 2018). Our study demonstrates that the amount of phengite in individual metamafic rock clasts can (theoretically) be quite large. It cannot, however, be estimated how much phengite overall is formed during such processes in other subduction systems. But seamounts depict substantial topographic irregularities on subducting oceanic plates and contribute to relief within the subduction channel, and it is well recognized that seamounts on outer-trench rises are deformed by faulting as the plate bends prior to subduction (e.g., Fryer & Smoot, 1985; Zhou & Lin, 2018). Subducting seamounts are subject to local increases in fluid pore pressure as they move through the subduction channel (e.g., Bell et al., 2010) and thus are prone to (further) deformation and possible decapitation (Watts et al., 2010). Although the detailed fate of deformation remains unclear (e.g., Wang & Bilek, 2014), it appears likely that much eroded material from subducted seamounts will be available for fluid–rock reactions (and fluid-induced metasomatism) in subduction channels/mélanges. With subduction channel thicknesses typically ranging from hundreds of meters to several kilometers (e.g., Cloos & Shreve, 1988; Guillot et al., 2009; Vannucchi et al., 2012) and the vast number of (eventually subducting) seamounts worldwide, it becomes clear that large masses of rock are likely to be compositionally (and mineralogically) modified. Bearing in mind the large stability field of phengite (Fig. 5b), we suppose that phengite formation in metamafics is potentially widespread throughout both cold and warm subduction zones.

Aside from being one of the major hosts for K in subduction environments, phengite is also known to incorporate high contents of fluid-mobile elements (e.g., Busigny et al., 2003; Bebout et al., 2013). Studies on high-*P* minerals in eclogitic rocks from the Central Alps have shown that phengite can accommodate >90% of the whole-rock budget of Rb, Cs, and Ba (Zack et al., 2001). Determining the trace elemental compositions of the metamorphic phases in the recycled OIBs is beyond the scope of this study, but bulk rock data imply enrichments in Rb, Cs, and to a lesser degree Th, as well as a markedly lower in Sr and Ba when compared to unsubducted Pacific seamounts (Fig. 8). The losses in Sr and Ba can be explained by the breakdown of Ca plagioclase and/or of clays during the subduction of the OIB (e.g., Putnis & John, 2010; Alt & Teagle, 2003). Gains in Rb and Cs can putatively—as those in K_2O and SiO_2—be ascribed to metasomatism in the subduction channel. Indeed, previous studies have shown that these fluid-mobile elements are mobilized in the Mariana forearc and concentrations in the fluids in the subduction channel are high (e.g., Wheat et al., 2018; Albers et al., 2020). We speculate that much of the Rb and Cs is hosted by phengite. This interpretation is in accordance with considerably higher amounts of Rb and Cs at Asùt Tesoru, relative to Fantangisña Seamount, from which phengite has primarily been reported (Ichiyama et al., 2021). Similarly, phengite in blueschist clasts from the South Chamorro Seamount, which has a similar depth-to-slab as Asùt Tesoru, has been shown to be the major carrier of slab-released fluid-mobile elements (B, Li, and Be; Pabst et al., 2012). The observed fluid-metasomatism, resulting in enhanced phengite formation, thus also has a direct bearing on trace element budgets.

Would such an increased formation of phengite have a bearing on the importance of phlogopite, the K–Mg mica that was suggested to have a major role in the cycling of K_2O and H_2O? Phlogopite crystallizes in the mantle wedge as a consequence of the infiltration of K-enriched slab-derived fluids. It decomposes at deeper levels where it releases H_2O that in turn triggers mantle wedge partial melting and hence contributes to back-arc magmatism (e.g., Peacock, 1990; Sudo & Tatsumi, 1990). The phlogopite breakdown reactions also release K_2O, generating K-rich magmas (e.g., Foley & Peccerillo, 1992; Condamine & Médard, 2014). However, Tamura et al. (2007) suggested that it is the breakdown of phengite that causes an increased mobility of K and consequently K-rich magmatism in the Izu–Bonin back-arc---whereas they attributed the scarcity of K-rich magmas in the arc-front to the presence and stability of phengite in the slab. Furthermore, other authors pointed out that phlogopite is not needed to generate K-rich melts (e.g., Wang et al., 2017). Our study highlights that the complexity of the subduction channel's mineralogy, which cannot be precisely defined. Potassium that is incorporated into phengite at shallow depths will unlikely be available to infiltrate the mantle wedge (to form phlogopite) somewhat deeper in the system. It remains unclear how much of the slab-released K is trapped in the subduction channel and how much of it can rise into/through the mantle wedge. Yet, at least at the forearc of the Mariana subduction zone, K-enriched fluids expelled by the serpentinite mud volcanoes provide evidence that the amount of K released from the slab outweighs that incorporated at depths. The formation of phlogopite deeper within the Mariana subduction system hence appears plausible. Indeed, incompatible trace element abundances and isotopic compositions of primitive magmas from the Mariana arc imply the presence of phlogopite in the source region (e.g., Tamura et al., 2014).

Conclusively, our geochemical data and thermodynamic models imply that elements are mobilized and redistributed soon after the subduction of AOC and sediments at the Mariana convergent margin. This redistribution of mass from phases that are only stable at low *P*/*T* into metamorphic/metasomatic minerals such as phengite and/or lawsonite, both stable until great depths, will affect geochemical cycling of major and trace elements deep within subduction zones. We have conceptualized these processes in Figure 9.

In the literature, contrasting reports persist on the degree of element mobility in shallow subduction settings. For example, Bebout & Barton (1993) reported on blueschist metabasaltic rocks from the Catalina Schist (Catalina Island, California) that exhibit K_2O enrichments up to >4 wt.%, accompanied by enrichments of Cs and Ba, and Shervais et al. (2011) documented prehnite–pumpellyite facies metavolcanics in a serpentinite mélange (Tehama–Colusa mélange, Coast Ranges, California) that are enriched in SiO_2 and Na_2O, but not K_2O. As demonstrated by Ghatak et al. (2012), however, metamafic rocks that experienced up to eclogite metamorphism largely preserved their protolith major and trace elemental compositions except for some fluid-mobile elements such as Ba, Pb, and to a smaller extent La, U, and Sr. More generally, Harlov & Austrheim (2013) summarized that subducting sediments and probably also igneous crustal rocks can largely retain their inventories of even the more fluid-mobile elements to at least 90 km in relatively cool subduction zones; higher geothermal gradients may generate greater forearc devolatilization leading to greater loss of fluids and fluid-mobile elements to the mantle wedge. They further stated that, at forearc depths, only the extremely mobile elements (for instance B, Cs, As, and Sb for the blueschist metasedimentary suite of the Catalina Schist) show a clear record of whole-rock loss, as based on comparisons between higher-grade rocks with lower-grade or unmetamorphosed equivalents.

A number of factors may influence the liberation of elements as well as metasomatic processes occurring soon after subduction, including the composition and state of the incoming lithosphere (i.e., type and thickness of sediment, nature and degree of alteration of the oceanic basement) or the thermal structure of the system. The variety of these in subduction zones worldwide may lead to decreased element mobility in some and elevated mobility in other sites. Further, the position of subducting rock within the convergent margin—it could metamorphose/metasomatize as part of the intact volcanic basement, could be positioned in the vicinity of a fluid conduit, or float within the subduction channel—is an important additional factor that contributes to the variability of element mobility (see discussion and references in Spandler & Pirard, 2013). Within the intact basement, rocks potentially mostly dehydrate at low f/r ratios and are being depleted in fluid-mobile elements (that are, once released, transported towards the upper plate). Since the subducting lithosphere provides a vast reservoir, large amounts of fluids and elements will be mobilized even though the elemental losses in individual rocks may appear minor and imply subduction metamorphism in a (more or less) closed system. Rocks situated along fluid pathways or in the subduction channel mélange, however, interact with slab-fluids at higher f/r ratios, leading to more increased modifications.

In the Mariana forearc, the extensive fluid–rock reactions in the subduction channel are particularly well documented. Enrichments (or depletion) of certain elements in rock clasts (this study; see also, e.g., Johnson, et al., 2014; Kahl et al., 2015; Tamblyn et al., 2019; Albers et al., 2020) allowed reconstructing processes in the subducting slab and during the fluids' rise toward the forearc seafloor. Serpentinites, for instance, incorporate fluid-mobile elements (Wei et al., 2005; Savov et al., 2007; Debret et al., 2019). Yet, despite high concentrations of these in the rocks, fluids emanating at the mud volcano summits still are considerably enriched in the same elements, implying that the mobilized amounts of these exceed what serpentinites can take up. Considering the putatively vast volumes of serpentinite produced in the Mariana forearc (e.g., Cai et al., 2018), the amount of mass mobilized from the slab must be immense. Several decades of research at the serpentinite mud volcanoes has clearly pointed out the significance of the liberation and transfer of fluids and mass at subduction depths <30 km. In line with these results, Kastner et al. (2014) estimated the global return flux of fluids and solutes from forearcs to the ocean through seeps and fault-controlled conduits to be large enough to importantly impact seawater chemistry (e.g., Mg, Ca, SO_4, and others).

Mass transfer and associated metasomatic processes that set in at shallow forearc depths are, however, often overlooked when geochemical cycling in subduction zones is investigated. Many (modeling) studies, for example, compare subduction inputs to arc volcanic outputs without considering metasomatism-related phase transitions. Our results strongly suggest that, for a holistic view, these processes need to be integrated. In line with these implications, previous studies concluded that up to kilometer-thick mélange zones in the subduction channel (formed during the mechanical mixing of materials from the subducting and overriding plates) may ultimately control the nature and composition of slab-derived fluids that enter the mantle wedge (e.g., King et al., 2006; Marschall & Schumacher, 2012; see also Spandler & Pirard, 2013).

5 Summary and conclusions

Data and models presented here provide insight regarding fluid-induced mass transfer and metasomatism within the shallow depths of an active subduction zone. We demonstrate that subducted OIB clasts have undergone substantial compositional changes, most likely at conditions that did not largely exceed 7–8 kbar and 200–350°C. Most noticeable and consistent throughout all clasts are enrichments in K_2O and H_2O, accompanied by SiO_2, Na_2O, and MgO gains in samples from Fantangisña Seamount and SiO_2 gains but MgO and Fe_2O_3* losses in samples from Asùt Tesoru Seamount. In addition, the fluid-mobile elements Cs and Rb are increased whereas Ba and Sr contents are decreased in all samples.

The metasomatic changes can be explained by the interaction of element-laden, slab-derived fluids with (fragmented) parts of subducted seamounts in the subduction channel. Our reaction path models predict the release of fluids enriched in K and other solutes from subducting oceanic lithosphere even at $T < 200$°C, consistent with known compositions of slab-derived fluids at the forearc seafloor. A K_2O-increase in OIB during its reaction with the above fluid is thermodynamically feasible.

The observed changes in major element composition have considerable ramifications for the clasts' metamorphic phase assemblages. Our equilibrium assemblage diagrams predict a strikingly increased stability field and much greater absolute amounts of phengite (up to four times as much) relative to unmetasomatized OIB. Phengite in turn can carry K_2O, H_2O, and fluid-mobile elements beyond sub-arc depths.

These results highlight the importance of acknowledging subduction processes at shallow depths (<30 km) as they may play a fundamental role in controlling *which* components as well as *in which state* (i.e., bound in which minerals) these components ultimately reach greater depths where they may or may not contribute to arc magmatism. It is most probable that the shallow processes observed here and/or similar ones also take place in all subduction zones.

6 Conflict of Interest

The authors declare that the research was conducted in the absence of any commercial or financial relationships that could be construed as a potential conflict of interest.

7 Author Contributions

EA, JS, YI, and PF sailed IODP Exp. 366. EA planned and designed the study. YI and EA examined the samples petrographically; bulk rock analyses were conducted by JS. EA performed thermodynamic calculations; CTH and EA compiled the thermodynamic database for EQ3/6. The manuscript was written by EA with contributions of all co-authors.

8 Funding

EA acknowledges funding by the Special Priority Program 527 'International Ocean Discovery Program' of the German Research Foundation (DFG), grant BA 1605/18–1, and by the Helmholtz Association 'POSY – The Polar System and its Effects on the Ocean Floor' (project no. ExNet-0001-Phase2-3). PF acknowledges funding by IODP-US Science Support Program.

9 Acknowledgments

This research used samples and data provided by IODP. We are grateful to the captain and crew of the D/V JOIDES Resolution, to the IODP science technicians, and to the Exp. 366 Science Party.

10 References

Albers, E.; Bach, W.; Klein, F.; Menzies, C. D.; Lucassen, F. & Teagle, D. A. H., 2019, Fluid–rock interactions in the shallow Mariana forearc: carbon cycling and redox conditions, *Solid Earth, 10*, 907-930, doi:10.5194/se-10-907-2019

Albers, E.; Kahl, W.-A.; Beyer, L. & Bach, W., 2020, Variant across-forearc compositions of slab-fluids recorded by serpentinites: implications on the mobilization of FMEs from an active subduction zone (Mariana forearc), *Lithos, 364–365*, 105525, doi:10.1016/j.lithos.2020.105525

Alt, J. C., 1995, Subseafloor processes in mid-ocean ridge hydrothermal systems, *Geophys. Monogr. Ser.*, *91*, 85–114, doi:10.1029/gm091p0085

Alt, J. C. & Teagle, D. A. H., 2003, Hydrothermal alteration of upper oceanic crust formed at a fast-spreading ridge: mineral, chemical, and isotopic evidence from ODP Site 801, *Chem. Geol., 201*, 191–211, doi:10.1016/S0009-2541(03)00201-8

Bach, W.; Jöns, N. & Klein, F., 2013, Metasomatism within the ocean crust, in: Harlov, D. E. & Austrheim, H. (eds.) Metasomatism and the chemical transformation of rock, Lecture notes in Earth system sciences, Springer, Berlin, Heidelberg, doi:10.1007/978-3-642-28394-9_8

Baker, P. E.; Castillo, P. R. & Condliffe, E., 1995, Petrology and geochemistry of igneous rocks from Allison and Resolution Guyots, Sites 865 and 866, in: Winterer, E. L., Sager, W. W., Firth, J. V. & Sinton, J. M. (eds.), Proc. ODP., Sci. Results, 143: College Station, TX (Ocean Drilling Program), doi:10.2973/odp.proc.sr.143.216.1995

Baldwin J. A.; Powell, R.; Brown, M.; Moraes, R. & Fuck, R. A., 2005, Modelling of mineral equilibria in ultrahigh-temperature metamorphic rocks from the Anapolis–Itaucu Complex, central Brazil, *J. Metamorph. Geol.*, *23*, 511–531, doi:10.1111/j.1525-1314.2005.00591.x

Bebout, G. E. & Barton, M. D., 1993, Metasomatism during subduction: products and possible paths in the Catalina Schist, California, *Chem. Geol., 108*, 61–92, doi:10.1016/0009-2541(93)90318-d

Bebout, G. E.; Ryan, J. G.; Leeman, W. P. & Bebout, A. E., 1999, Fractionation of trace elements by subduction-zone metamorphism—effect of convergent-margin thermal evolution, *Earth Planet. Sci. Lett., 171*, 63–81, doi:10.1016/s0012-821x(99)00135-1

Bebout, G. E.; Agard, P.; Kobayashi, K.; Moriguti, T. & Nakamura, E., 2013, Devolatilization history and trace element mobility in deeply subducted sedimentary rocks: evidence from Western Alps HP/UHP suites, *Chem. Geol., 342*, 1–20, doi:10.1016/j.chemgeo.2013.01.009

Bekins, B.; McCaffrey, A. M. & Dreiss, S. J., 1994, Influence of kinetics on the smectite to illite transition in the Barbados accretionary prism, *J. Geophys. Res. Solid Earth, 99*, 18147–18158, doi:10.1029/94jb01187

Bell, R.; Sutherland, R.; Barker, D. H. N.; Henrys, S.; Bannister, S.; Wallace, L. & Beavan, J., 2010, Seismic reflection character of the Hikurangi subduction interface, New Zealand, in the region of repeated Gisborne slow slip events, *Geophys. J. Int.*, *180*, 34–48, doi:10.1111/j.1365-246x.2009.04401.x

Busigny, V.; Cartigny, P.; Philippot, P.; Ader, M. & Javoy, M., 2003, Massive recycling of nitrogen and other fluid-mobile elements (K, Rb, Cs, H) in a cold slab environment: evidence from HP to UHP oceanic metasediments of the Schistes Lustrés nappe (western Alps, Europe), *Earth Planet. Sci. Lett., 215*, 27–42, doi:10.1016/s0012-821x(03)00453-9

Cai, C.; Wiens, D. A.; Shen, W. & Eimer, M., 2018, Water input into the Mariana subduction zone estimated from ocean-bottom seismic data, *Nature, 563*, 389–392, doi:10.1038/s41586-018-0655-4

Chen, S.; Guo, X.; Yoshino, T.; Jin, Z. & Li, P., 2018, Dehydration of phengite inferred by electrical conductivity measurements: implication for the high conductivity anomalies relevant to the subduction zones, *Geology, 46*, 11–14, doi:10.1130/g39716.1

Cloos, M. & Shreve, R. L., 1988, Subduction-channel model of prism accretion, mélange formation, sediment subduction, and subduction erosion at convergent plate margins: 1. Background and description, *Pure Appl. Geophys.*, *128*, 455–500, doi: 10.1007/bf00874548

Codillo, E. A.; Le Roux, V. & Marschall, H. R., 2018, Arc-like magmas generated by mélange-peridotite interaction in the mantle wedge, *Nat. Commun., 9*, 2864, doi:10.1038/s41467-018-05313-2

Condamine, P. & Médard, E., 2014, Experimental melting of phlogopite-bearing mantle at 1 GPa: implications for potassic magmatism, *Earth Planet. Sci. Lett.*, *397*, 80–92, doi:10.1016/j.epsl.2014.04.027

Davis, A. S.; Pringle, M. S.; Pickthorn, L.-B. G. & Clague, D. A., 1989, Petrology and age of alkalic lava from the Ratak Chain of the Marshall Islands, *J. Geophys. Res.*, *94*, 5757–5774, doi:10.1029/jb094ib05p05757

de Capitani, C. & Brown, T. H., 1987, The computation of chemical equilibrium in complex systems containing non-ideal solutions, *Geochim. Cosmochim. Acta*, *51*, 2639–2652, doi:10.1016/0016-7037(87)90145-1

de Capitani, C. & Petrakakis, K., 2010, The computation of equilibrium assemblage diagrams with Theriak/Domino software, *Am. Mineral.*, *95*, 1006–1016, doi:10.2138/am.2010.3354

Debret, B.; Albers, E.; Walter, B.; Price, R.; Barnes, J. D.; Beunon, H.; Facq, S.; Gillikin, D. P.; Mattielli, N. & Williams, H., 2019, Shallow forearc mantle dynamics and geochemistry: new insights from IODP Expedition 366, *Lithos, 326–327*, 230–245, doi:10.1016/j.lithos.2018.10.038

Deng, J.; Zhang, L.; Liu, H.; Liu, H.; Liao, R.; Mastoi, A. S.; Yang, X. & Sun, W., 2021, Geochemistry of subducted metabasites from the Mariana forearc: implications for Pacific seamount subduction, *Geosci. Front.*, *12*, 101117, doi:10.1016/j.gsf.2020.12.002

Deschamps, F.; Guillot, S.; Godard, M.; Andreani, M. & Hattori, K., 2011, Serpentinites act as sponges for fluid-mobile elements in abyssal and subduction zone environments, *Terra Nova, 23*, 171–178, doi:10.1111/j.1365-3121.2011.00995.x

Ernst, W. G., 1984, Californian blueschists, subduction, and the significance of tectonostratigraphic terranes, *Geology*, *12*, 436–440, doi:10.1130/0091-7613(1984)12<436:cbsats>2.0.co;2

Foley, S. & Peccerillo, A., 1992, Potassic and ultrapotassic magmas and their origin, *Lithos*, *28*, 181–185, doi:10.1016/0024-4937(92)90005-j

Fryer, P. B., 2012, Serpentinite mud volcanism: observations, processes, and implications, *Ann. Rev. Mar. Sci., 4*, 345–373, doi:10.1146/annurev-marine-120710-100922

Fryer, P. & Smoot, N. C., 1985, Processes of seamount subduction in the Mariana and Izu-Bonin Trenches, *Marine Geology*, *64*, 77–90, doi:10.1016/0025-3227(85)90161-6

Fryer, P.; Ambos, E. L. & Hussong, D. M., 1985, Origin and emplacement of Mariana forearc seamounts, *Geology*, *13*, 774–777, doi:10.1130/0091-7613(1985)13<774:oaeomf>2.0.co;2

Fryer, P., Pearce, J. A., Stokking, L. B., et al., 1992, Proc. ODP, Sci. Results, 125: College Station, TX (Ocean Drilling Program), doi:10.2973/odp.proc.sr.125.1992

Fryer, P.; Mottl, M.; Johnson, L.; Haggerty, J.; Phipps, S. & Maekawa, H., 1995, Serpentine bodies in the forearcs of western Pacific convergent margins: origin and associated fluids, *Geophys. Monogr. Ser.*, *88*, 259–279, doi:10.1029/gm088p0259

Fryer, P.; Gharib, J.; Ross, K.; Savov, I. & Mottl, M. J., 2006, Variability in serpentinite mudflow mechanisms and sources: ODP drilling results on Mariana forearc seamounts, *Geochem. Geophys. Geosyst., 7*, Q08014, doi:10.1029/2005gc001201

Fryer, P.; Wheat, C. G.; Williams, T. & the Expedition 366 Scientists, 2018, Mariana convergent margin and South Chamorro Seamount, Proc. IODP, 366: College Station, TX (International Ocean Discovery Program), doi:10.14379/iodp.proc.366.101.2018

Fryer, P.; Wheat, C.; Williams, T.; Kelley, C.; Johnson, K.; Ryan, J.; Kurz, W.; Shervais, J.; Albers, E.; Bekins, B.; Debret, B.; Deng, J.; Dong, Y.; Eickenbusch, P.; Frery, E.; Ichiyama, Y.; Johnston, R.; Kevorkian, R.; Magalhaes, V.; Mantovanelli, S.; Menapace, W.; Menzies, C.; Michibayashi, K.; Moyer, C.; Mullane, K.; Park, J.-W.; Price, R.; Sissman, O.; Suzuki, S.; Takai, K.; Walter, B.; Zhang, R.; Amon, D.; Glickson, D. & Pomponi, S., 2020, Mariana serpentinite mud volcanism exhumes subducted seamount materials: implications for the origin of life, *Phil. Trans. R. Soc. A, 378*, 20180425, doi:10.1098/rsta.2018.0425

Geilert, S.; Grasse, P.; Wallmann, K.; Liebetrau, V. & Menzies, C. D., 2020, Serpentine alteration as source of high dissolved silicon and elevated δ^{30}Si values to the marine Si cycle, *Nat. Commun.*, *11*, 5123, doi:10.1038/s41467-020-18804-y

Geilert, S.; Albers, E.; Frick, D. A.; Hansen, C. T. & von Blanckenburg, F., 2021, Systematic changes in serpentine Si isotope signatures across the Mariana forearc – a new proxy for slab dehydration processes, *Earth Planet. Sci. Lett.*, *575*, 117193, doi:10.1016/j.epsl.2021.117193

Ghatak, A.; Basu, A. R. & Wakabayashi, J., 2012, Elemental mobility in subduction metamorphism: insight from metamorphic rocks of the Franciscan Complex and the Feather River ultramafic belt, California, *Int. Geol. Rev., 54*, 654–685, doi:10.1080/00206814.2011.567087

Giaramita, M.; MacPherson, G. J. & Phipps, S. P., 1988, Petrologically diverse basalts from a fossil oceanic forearc in California: the Llanada and Black Mountain remnants of the Coast Range ophiolite, *Geol. Soc. Am. Bull.*, *110*, 553–571, doi:10.1130/0016-7606(1998)110<0553:pdbfaf>2.3.co;2

Grant, J. A., 1986, The isocon diagram—a simple solution to Gresens' equation for metasomatic alteration, *Econ. Geol.*, *81*, 1976–1982, doi:10.2113/gsecongeo.81.8.1976

Gresens, R. L., 1967, Composition–volume relationships of metasomatism, *Chem. Geol.*, *2*, 47–65, doi:10.1016/0009-2541(67)90004-6

Guillot, S.; Hattori, K; Agard, P.; Schwarz, S. & Vidal, O., 2009, Exhumation processes in oceanic and continental subduction contexts: a review, in: Lallemand, S. & Funiciello, F. (eds.) *Subduction zone geodynamics*, Springer, Berlin Heidelberg, doi:10.1007/978-3-540-87974-9

Harlov, D. E. & Austrheim, H., 2013, Metasomatism and the chemical transformation of rock: the role of fluids in terrestrial and extraterrestrial processes, *Springer,* Berlin/Heidelberg, doi:10.1007/978-3-642-28394-9

Holland, T. J. B. & Powell, R., 1998, An internally consistent thermodynamic dataset for phases of petrological interest, *J. Metamorph. Geol.*, *16*, 309–343, doi:10.1111/j.1525-1314.1998.00140.x

Holland, T. J. B. & Powell, R., 2003, Activity-composition relations for phases in petrological calculations: an asymmetric multicomponent formulation, *Contrib. Mineral. Petrol.*, *145*, 492–501, doi:10.1007/s00410-003-0464-z

Holland, T. J. B. & Powell, R., 2011, An improved and extended internally consistent thermodynamic dataset for phases of petrological interest, involving a new equation of state for solids, *J. Metamorph. Geol.*, *29*, 333–383, doi:10.111/j.1525-1314.2010.00923.x

Hulme, S. M.; Wheat, C. G.; Fryer, P. B. & Mottl, M. J., 2010, Pore water chemistry of the Mariana serpentinite mud volcanoes: a window to the seismogenic zone, *Geochem. Geophys. Geosyst., 11*, Q01X09, doi:10.1029/2009gc002674

Ichiyama, Y.; Tsujimori, T.; Fryer, P.; Michibayashi, K.; Tamura, A. & Morishita, T., 2021, Temporal and spatial mineralogical changes in clasts from Mariana serpentinite mud volcanoes: cooling of the hot forearc-mantle at subduction initiation, *Lithos, 384–385*, 105941, doi:10.1016/j.lithos.2020.105941

Jackson, M. G. & Dasgupta, R., 2008, Compositions of HIMU, EM1, and EM2 from global trends between radiogenic isotopes and major elements in ocean island basalts, *Earth Planet. Sci. Lett.*, *276*, 175–186, doi:10.1016/j.epsl.2008.09.23

Janney, P. E. & Castillo, P. R., 1999, Isotope geochemistry of the Darwin Rise seamounts and the nature of long-term mantle dynamics beneath the south central Pacific, *J. Geophys. Res.*, *104*, 10,571–10,589, doi:10.1029/1998jb900061

Jayko, A. S.; Blake, M. C. & Brothers, R. N., 1986, Blueschist metamorphism of the Eastern Franciscan belt, northern California, *Geol. Soc. Am. Mem.*, *164*, 107–123, doi:10.1130/mem164-p107

Johnson, J. A.; Hickey-Vargas, R.; Fryer, P.; Salters, V. & Reagan, M. K., 2014, Geochemical and isotopic study of a plutonic suite and related early volcanic sequences in the southern Mariana forearc, *Geochem. Geophys. Geosyst.*, *15*, 589–604, doi:10.1002/2013gc005053

Kahl, W.-A.; Jöns, N.; Bach, W.; Klein, F. & Alt, J. C., 2015, Ultramafic clasts from the South Chamorro serpentine mud volcano reveal a polyphase serpentinization history of the Mariana forearc mantle, *Lithos, 227*, 1–20, doi:10.1016/j.lithos.2015.03.015

Kastner, M.; Solomon, E. A.; Harris, R. N. & Torres, M. E., 2014, Fluid origins, thermal regimes, and fluid and solute fluxes in the forearc of subduction zones, in: Stein, R.; Blackman, D. K.; Inagaki, F. & Larsen, H.-C. (eds.), *Earth and life processes discovered from subseafloor environments: a decade of science achieved by the Integrated Ocean Drilling Program (IODP), Elsevier, 7*, 671–733, doi:10.1016/b978-0-444-62617-2.00022-0

Kelley, K. A.; Plank, T.; Ludden, J. & Staudigel, H., 2003, Composition of altered oceanic crust at ODP Sites 801 and 1149, *Geochem. Geophys. Geosyst., 4*, 8910, doi:10.1029/2002gc000435

King, R.; Bebout, G.; Moriguti, R. & Nakamura, E., 2006, Elemental mixing systematics and Sr–Nd isotope geochemistry of mélange formation: obstacles to identification of fluid sources to arc volcanics, *Earth Planet. Sci. Lett., 246*, 288–304, doi:10.1016/j.epsl.2006.03.053

Koppers, A. A. P.; Staudigel, H.; Wijbrans, J. R. & Pringle, M. S., 1998, The Magellan Seamount Trail: implications for Cretaceous hotspot volcanism and absolute Pacific Plate motion, *Earth Planet. Sci. Lett.*, *163*, 53–68, doi:10.1016/s0012-821x(98)00175-7

Leat, P. T. & Larter, R. D., 2003, Intra-oceanic subduction systems: introduction, *Geol. Soc. Spec. Pub., 219*, 1–17, doi:10.1144/gsl.sp.2003.219.01.01

Liu, Y.; Zhang, G.; Zhang, J. & Wang, S., 2020, Geochemical constraints on CO_2-rich mantle source for the Kocebu Seamount, Magellan Seamount chain in the western Pacific, *J. Oceanol. Limnol.*, *38*, 1201–1214, doi:10.1007/s00343-020-0013-x

Lockwood, J. P., 1972, Possible mechanisms for the emplacement of alpine-type serpentinite, *Geol. Soc. Am. Mem.*, 132, 273–288, doi:10.1130/mem132-p273

Maekawa, H.; Masaya, S.; Ishill, T.; Fryer, P. & Pearce, J. A., 1993, Blueschist metamorphism in an active subduction zone, *Nature, 364*, 520–523, doi:10.1038/364520a0

Manning, C. E., 2004, The chemistry of subduction-zone fluids, *Earth Planet. Sci. Lett., 223*, 1–16, doi:10.1016/j.epsl.2004.04.030

Marschall, H. R. & Schumacher, J. C., 2012, Arc magmas sourced from mélange diapirs in subduction zones, *Nat. Geosci., 5*, 862–867, doi:10.1038/ngeo1634

Menzies, C.; Price, R. E.; Ryan, J.; Sissman, O.; Takai, K.; Wheat, C G., 2021, Spatial variation of subduction zone fluids during progressive subduction: insights from Serpentinite mud volcanoes, *Geochim. Cosmochim. Acta*, in press, doi:10.1016/j.gca.2021.10.030

Moore, J. C. & Vrolijk, P., 1992, Fluids in accretionary prisms, *Rev. Geophys., 30*, 113–135, doi:10.1029/92rg00201

Mottl, M. J.; Wheat, C. G.; Fryer, P. B.; Gharib, J. & Martin, J. B., 2004, Chemistry of springs across the Mariana forearc shows progressive devolatilization of the subducting plate, *Geochim. Cosmochim. Acta, 68*, 4915–4933, doi:10.1016/j.gca.2004.05.037

Oakley, A. J., 2008, A multi-channel seismic and bathymetric investigation of the central Mariana convergent margin, *PhD Thesis*, University of Hawai'i, Manoa, HI

Oakley, A. J.; Taylor, B. & Moore, G. F., 2008, Pacific Plate subduction beneath the central Mariana and Izu-Bonin fore arcs: new insights from an old margin, *Geochem. Geophys. Geosyst., 9*, Q06003, doi:10.1029/2007gc001820

Pabst, S.; Zack, T.; Savov, I. P.; Ludwig, T.; Rost, D.; Tonarini, S. & Vicenzi, E. P., 2012, The fate of subducted oceanic slabs in the shallow mantle: insights from boron isotopes and light element composition of metasomatized blueschists from the Mariana forearc, *Lithos, 132–133*, 162–179, doi:10.1016/j.lithos.2011.11.010

Pattison, D. R. M.; De Capitani, C. & Gaidies, F., 2011, Petrological consequences of variations in metamorphic reaction affinity, *J. Metamorph. Geol., 29*, 953–977, doi:10.1111/j.1525-1314.2011.00950.x

Peacock, S. A., 1990, Fluid processes in subduction zones, *Science, 248*, 329–337, doi:10.1126/science.248.4953.329

Peacock, S. A. & Wang, K., 1999, Seismic consequences of warm versus cool subduction metamorphism: examples from Southwest and Northeast Japan, *Science*, *286*, 937–939, doi:10.1126/science.286.5441.937

Perfit, M. R.; Gust, D. A.; Bence, A. E.; Arculus, R. J. & Taylor, S. R., 1980, Chemical characteristics of island-arc basalts: implications for mantle sources, *Chem. Geol., 30*, 227–256, doi:10.1016/0009-2541(80)90107-2

Plank, T. & Langmuir, C. H., 1998, The chemical composition of subducting sediment and its consequences for the crust and mantle, *Chem. Geol., 145*, 325–394, doi:10.1016/s0009-2541(97)00150-2

Plank, T.; Ludden, J. N.; Escutia, C. & et al., 2000, *Proc. ODP 185, Ocean Drilling Program, TX,* doi:10.2973/odp.proc.ir.185.2000

Poli, S. & Schmidt, M. W., 1995, H_2O transport and release in subduction zones: experimental constraints on basaltic and andesitic systems, *J. Geophys. Res. Solid Earth, 100*, 22299–22314, doi:10.1029/95jb01570

Pons, M.-L.; Quitté, G.; Fujii, T.; Rosing, M. T.; Reynard, B.; Moynier, F.; Douchet, C. & Albarède, F., 2011, Early Archean serpentine mud volcanoes at Isua, Greenland, as a niche for early life, *Proc. Natl. Aca. Sci.*, 108, 17639–17643, doi:10.1073/pnas.1108061108

Putnis, A. & Austrheim, H., 2010, Fluid-induced processes: metasomatism and metamorphism, *Geofluids, 10*, 254–269, doi:10.1111/j.1468-8123.2010.00285.x

Putnis, A. & John, T., 2010, Replacement processes in the Earth's crust, *Elements, 6*, 159–164, doi:10.2113/gselements.6.3.159

Ringwood, A. E., 1969, Composition and evolution of the upper mantle, *Geoph. Monog. Series, 13*, 1–17, doi:10.1029/gm013p0001

Rustioni, G.; Audetat, A. & Keppler, H., 2021, The composition of subduction zone fluids and the origin of the trace element enrichments in arc magmas, *Contrib. Mineral. Petrol.*, *176*, 51, doi:10.1007/s00410-021-01810-8

Savov, I. P.; Guggino, S.; Ryan, J. G.; Fryer, P. B. & Mottl, M. J., 2005a, Geochemistry of serpentinite muds and metamorphic rocks from the Mariana forearc, ODP Sites 1200 and 778–779, South Chamorro and Conical Seamounts, in: Shinohara, M.; Salisbury, M. H. & Richter, C. *(Eds.), Proc. ODP 195, Sci. Results*, *195*, 1–49, doi:10.2973/odp.proc.sr.195.103.2005

Savov, I. P.; Ryan, J. G.; Antonio, M. D.; Kelley, K. & Mattie, P., 2005b, Geochemistry of serpentinized peridotites from the Mariana forearc Conical Seamount, ODP Leg 125: implications for the elemental recycling at subduction zones, *Geochem. Geophys. Geosyst., 6*, Q04J15, doi:10.1029/2004gc000777

Savov, I. P.; Ryan, J. G.; Antonio, M. D. & Fryer, P., 2007, Shallow slab fluid release across and along the Mariana arc-basin system: insights from geochemistry of serpentinized peridotites from the Mariana fore arc, *J. Geophys. Res., 112*, B09205, doi:10.1029/2006jb004749

Scambelluri, M. & Philippot, P., 2001, Deep fluids in subduction zones, *Lithos, 55*, 213–227, doi:10.1016/s0024-4937(00)00046-3

Schmidt, M. W., 1996, Experimental constraints on recycling of potassium from subducted oceanic crust, *Science, 272*, 1927–1930, doi:10.1126/science.272.5270.1927

Shervais, J. W., 1982, Ti-V plots and the petrogenesis of modern and ophiolitic lavas, *Earth Planet. Sci. Lett., 59*, 101–118, doi:10.1016/0012-821x(82)90120-0

Shervais, J. W., 2021, The petrogenesis of modern and ophiolitic lavas reconsidered: Ti–V and Nb–Th, *Geosci. Front.*, in press, doi: 10.1016/j.gsf.2021.101319

Shervais, J. W.; Choi, S. H.; Sharp, W. D.; Ross, J.; Zoglman-Schuman, M. & Mukasa, S. B., 2011, Serpentinite matrix mélange: implications of mixed provenance for mélange formation, *Geol. Soc. Am. Spec. Pap.*, *480*, 1–38, doi:10.1130/2011.2480(01)

Shervais, J. W.; Reagan, M.; Haugen, E.; Almeev, R. R.; Pearce, J. A.; Prytulak, J.; Ryan, J. G.; Whattam, S. A.; Godard, M.; Chapman, T.; Li, H.; Kurz, W.; Nelson, W. R.; Heaton, D.; Kirchenbaur, M.; Shimizu, K.; Sakuyama, T.; Li, Y. & Vetter, S. K., 2019, Magmatic response to subduction initiation: part 1. Fore-arc basalts of the Izu-Bonin Arc from IODP Expedition 352, *Geochem. Geophys. Geosyst.*, *20*, 314–338, doi:10.1029/2018gc007731

Spandler, C. & Pirard, C., 2013, Element recycling from subducting slabs to arc crust: a review, *Lithos, 170*, 208–223, doi:10.1016/j.lithos.2013.02.016

Staudigel, H., 2014, Chemical fluxes from hydrothermal alteration of the oceanic crust, *Treatise on geochemistry, Elsevier,* 583–606, doi:10.1016/b978-0-08-095975-7.00318-1

Staudigel, H.; Plank, T.; White, B. & Schmincke, H.-U., 1996, Geochemical fluxes during seafloor alteration of the basaltic upper oceanic crust: DSDP Sites 417 and 418, *Geoph. Monog. Ser., 96*, 19–38, doi:10.1029/gm096p0019

Staudigel, H.; Koppers, A. A. P.; Plank, T. A. & Hanan, B. B., 2010, Seamounts in the subduction factory, *Oceanography*, *23*, 176–181, doi:10.5670/oceanog.2010.69

Stern, R. J., 2002, Subduction zones, *Rev. Geophys., 40*, 4, 1012, doi:10.1029/2001rg000108

Sudo, A. & Tatsumi, Y., 1990, Phlogopite and K-amphibole in the upper mantle: implications for magma genesis in subduction zones, *Geophys. Res. Lett.*, *17*, 29–32, doi:10.1029/gl017i001p00029

Sun, S.-s. & McDonough, W. F., 1989, Chemical and isotopic systematics of oceanic basalts: implications for mantle composition and processes, *Geological Society Special Publications, 42*, 313–345, doi:10.1144/gsl.sp.1989.042.01.19

Tamblyn, R.; Zack, T.; Schmitt, A. K.; Hand, M.; Kelsey, D.; Morrissey, L.; Pabst, S. & Savov, I. P., 2019, Blueschist from the Mariana forearc records long-lived residence of material in the subduction channel, *Earth Planet. Sci. Lett., 519*, 171–181, doi:10.1016/j.epsl.2019.05.013

Tamura, Y.; Tani, K.; Chang, Q.; Shukuno, H.; Kawabata, H.; Ishizuka, O. & Fiske, R. S., 2007, Wet and dry basalt magma evolution at Torishima Volcano, Izu–Bonin Arc, Japan: the possible role of phengite in the downgoing slab, *J. Petrol.*, *48*, 1999–2031, doi:10.1093/petrology/egm048

Tamura, Y.; Ishizuka, O.; Stern, R. J.; Nichols, A. R. L.; Kawabata, H.; Hirahara, Y.; Chang, Q.; Miyazaki, T.; Kimura, J.-I.; Embley, R. W. & Tatsumi, Y., 2014, Mission immiscible: distinct subduction components generate two primary magmas at Pagan Volcano, Mariana Arc, *J. Pet.*, *55*, 63–101, doi:10.1093/petrology/egt061

Tang, L.; Dong, Y.; Chu, F.; Chen, L.; Ma, W. & Liu, Y., 2019, Geochemistry and age of seamounts in the West Pacific: mantle processes and petrogenetic implications, *Acta Oceanol. Sin.*, *38*, 71–77, doi:10.1007/s13131-019-1371-0

Tatsumi, Y. & Eggins, S., 1995, Subduction zone magmatism, *Blackwell Science*, Cambridge

Taylor, S. R. & McLennan, S. M., 1995, The geochemical evolution of the continental crust, *Rev. Geophys., 33*, 241–265, doi:10.1029/95rg00262

Ukar, E. & Cloos, M., 2014, Low-temperature blueschist-facies mafic blocks in the Franciscan mélange, San Simeon, California: field relations, petrology, and counterclockwise *P-T* paths, *Geol. Soc. Am. Bull.*, *126*, 831–856, doi:10.1130/b30876.1

Ulmer, P., 2001, Partial melting in the mantle wedge—the role of H_2O in the genesis of mantle-derived 'arc-related' magmas, *Phys. Earth Planet. Inter., 127*, 215–232, doi:10.1016/s0031-9201(01)00229-1

Vannucchi, P.; Sage, F.; Phipps Morgan, J.; Remitti, F. & Collot, J.-Y., 2012, Toward a dynamic concept of the subduction channel at erosive convergent margins with implications for interplate material transfer, *Geochem. Geophys. Geosyst.*, *13*, Q02003, doi:10.1029/2011gc003846

Wang, K. & Bilek, S. L., 2014, Inited review paper: Fault creep caused by subduction of rough seafloor relief, *Tectonophysics*, *610*, 1–24, doi:10.1016/j.tecto.2013.11.024

Wang, Y.; Foley, S. F. & Prelević, D., 2017, Potassium-rich magmatism from a phlogopite-free source, *Geology*, *45*, 467–470, doi:10.1130/g38691.1

Watts, A. B.; Koppers, A. A. P. & Robinson, D. P., 2010, Seamount subduction and earthquakes, *Oceanography*, *23*, 166–173, doi: 10.5670/oceanog.2010.68

Wei, W.; Kastner, M.; Deyhle, A. & Spivack, A. J., 2006, Geochemical cycling of fluorine, chlorine, bromine, and boron and implications for fluid-rock reactions in Mariana forearc, South Chamorro Seamount, ODP Leg 195, in: Shinohara, M.; Salisbury, M. H.; Richter, C. (*Eds.*), *Proc. ODP*, *Sci. Results*, 195, 1–23, doi:10.2973/odp.proc.sr.195.106.2005

Wessel, P; Smith, W. H. F.; Scharroo, R.; Luis, J. & Wobbe, F., 2013, Generic Mapping Tools: improved version released, *Eos*, *94*, 409–410, doi:10.1002/2013eo450001

Wheat, C. G.; Fournier, T.; Paul, C.; Menzies, C.; Price, R. E.; Ryan, J. & Sissman, O., 2018, Data report: IODP Expedition 366 pore water trace elements (V, Mo, Rb, Cs, U, Ba, and Li) compositions, in: Fryer, P.; Wheat, C. G.; Williams, T. & the Expedition 366 Scientists, *Proc. IODP*, 366, doi:10.14379/iodp.proc.366.201.2018

White, R.W.; Powell, R. & Holland, T. J. B., 2007, Progress relating to calculation of partial melting equilibria for metapelites, *J. Metamorph. Geol.*, *25*, 511–527, doi:10.1111/j.1525-1314.2007.00711.x

White, R.W.; Powell, R. & Johnson, T. E., 2014a, The effect of Mn on mineral stability in metapelites revisited: new *a*–*x* relations for manganese-bearing minerals, *J. Metamorph. Geol.*, *32*, 809–828, doi:10.1111/jmg.12095

White, R.W.; Powell, R.; Holland, T. J. B.; Johnson, T. E. & Green, E. C. R., 2014b, New mineral activity–composition relations for thermodynamic calculations in metapelitic systems, *J. Metamorph. Geol.*, *32*, 261–286, doi:10.1111/jmg.12071

Zack, T.; Rivers, T. & Foley, S. F., 2001, Cs–Rb–Ba systematics in phengite and amphibole: an assessment of fluid mobility at 2.0 GPa in eclogites from Trescolmen, Central Alps, *Contrib. Mineral. Petrol.*, *140*, 651–669, doi:10.1007/s004100000206

Zhou, Z. & Lin, J., 2018, Elasto-plastic deformation and plate weakening due to normal faulting in the subducting plate along the Mariana Trench, *Tectonophysics*, *734–735*, 59–68, doi.org/10.1016/j.tecto.2018.04.008

11 Data Availability Statement

The original contributions presented in the study are included in the article; Supplementary Material will be available after the acceptance of the manuscript for publication. Further inquiries can be directed to the corresponding author.

Figures

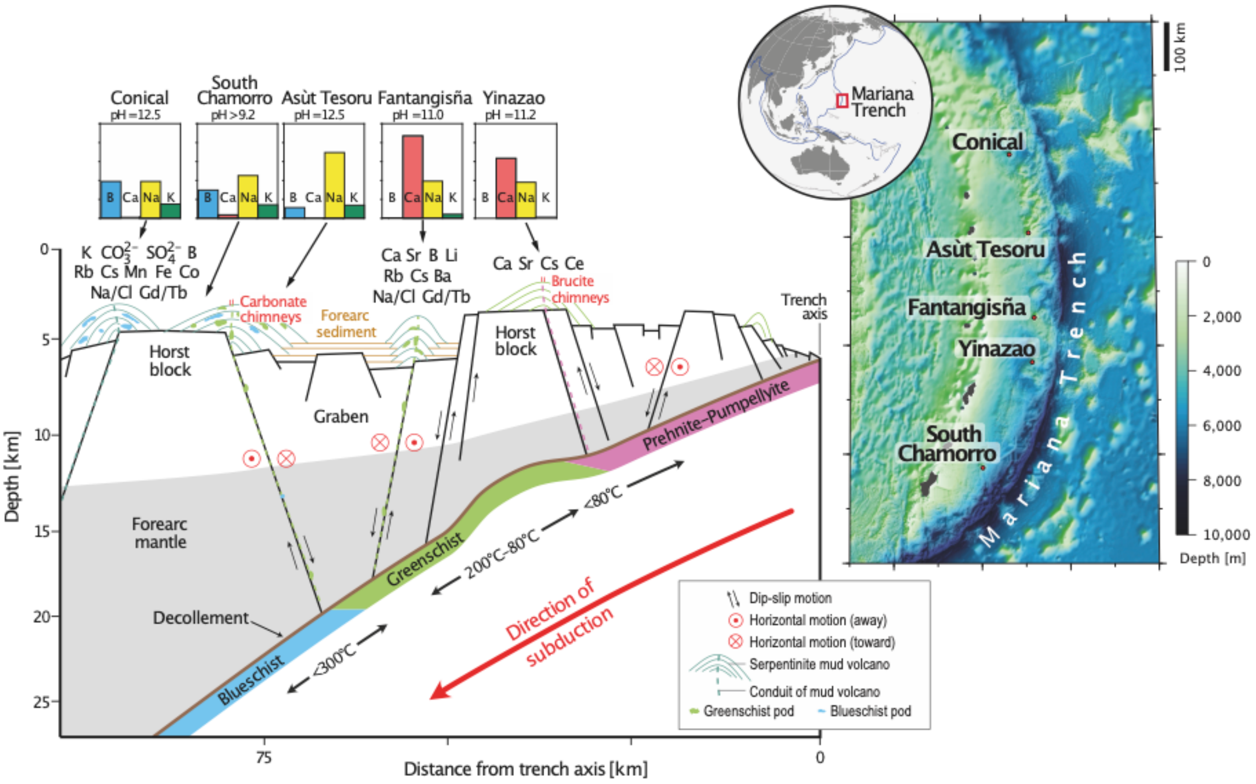

Figure 1: Idealized cross section of the Mariana forearc setting, from east to west, including the relative positioning of the serpentinite mud volcanoes. Compositions of the slab-derived serpentinite mud pore waters systematically vary across the forearc, reflecting prograde metamorphic processes in the subducting slab. The map shows the distribution of the serpentinite mud volcanoes drilled by ODP and IODP on the Mariana forearc. Also note the large number of Pacific seamounts that will eventually be subducted. Modified from Fryer et al. (2018) and Wheat et al. (2018). Globe inset and map created with Generic Mapping Tools (Wessel et al., 2013) with the Mariana Trench 6 arc-second Bathymetric Digital Elevation Model from the NOAA's National Geophysical Data Center.

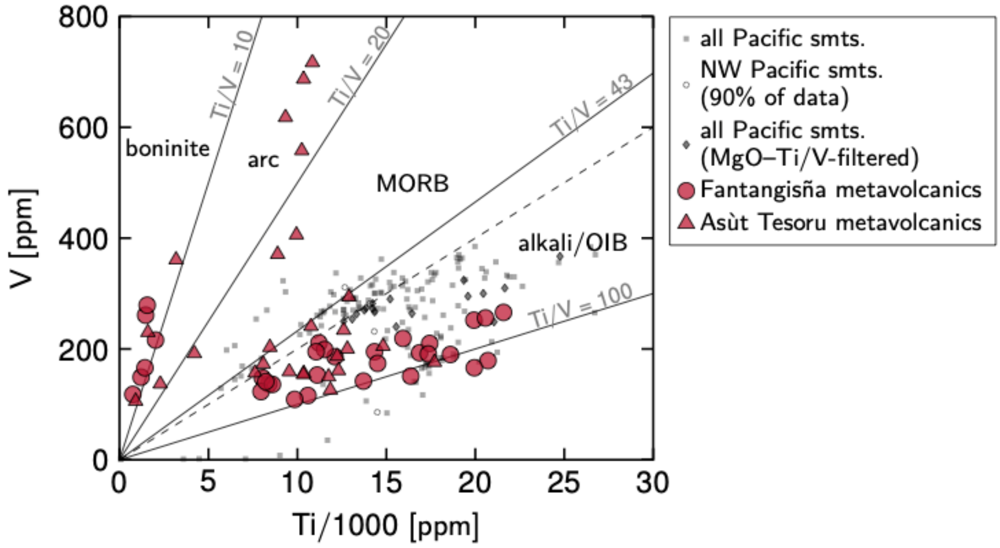

Figure 2: Bulk rock Ti–V systematics of metamafic clasts recovered during IODP Exp. 366. An OIB provenance is implied by Ti/V ratios between 43 and 100 (Shervais, 2021; the dashed line marks the now revised discrimination line of Ti/V = 50 after Shervais, 1982) for the clasts from Fantangisña and Asùt Tesoru Seamounts that are discussed in this paper. Data from Fryer et al. (2020) and Deng et al. (2021). Compositions of Pacific seamounts are shown for comparison (see Section 2.1 for more information and data sources).

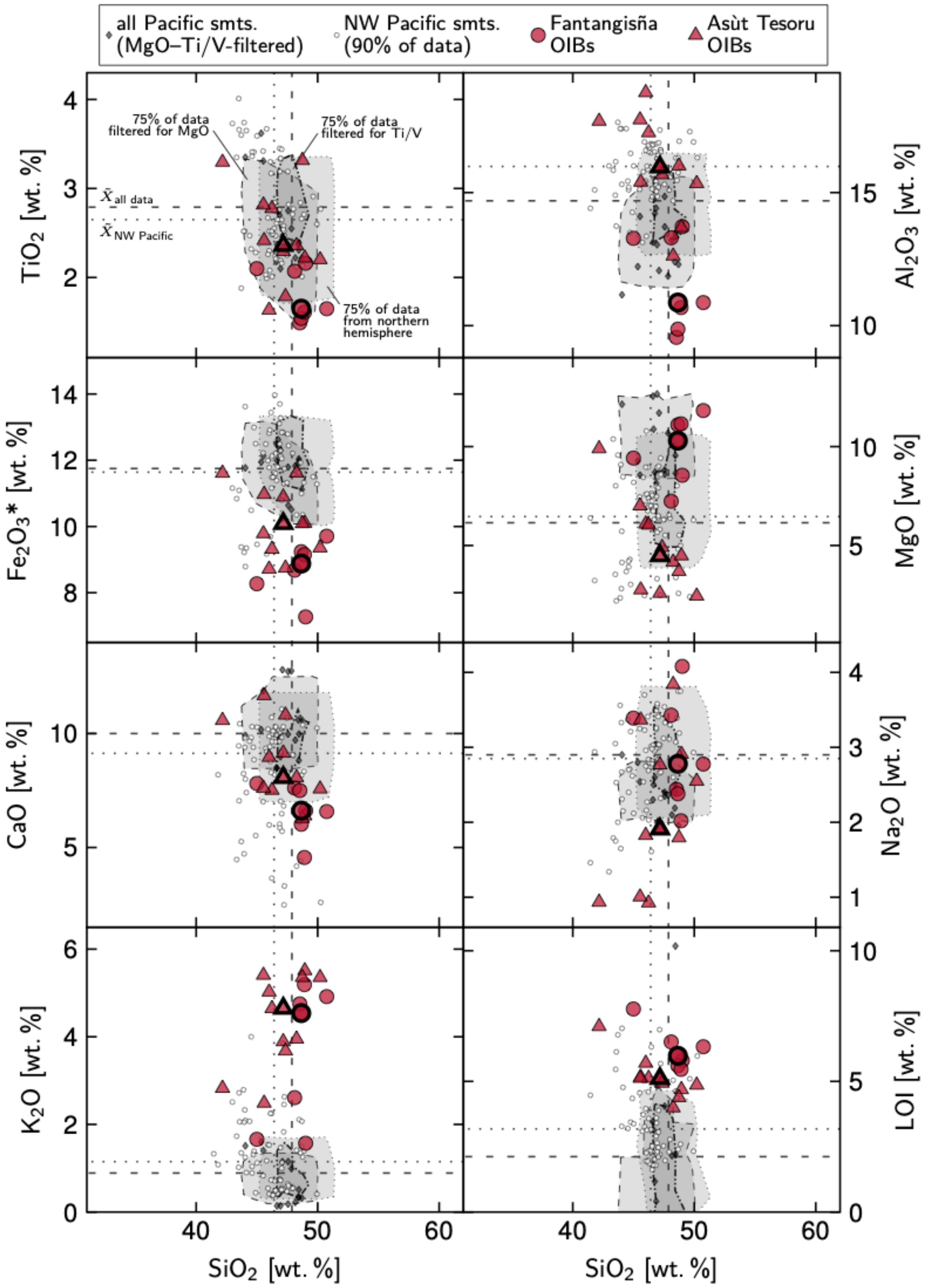

Figure 3: Bulk compositions of recycled OIBs from Fantangisña and Asùt Tesoru Seamounts presented in a Harker diagram. Marks with thick outlines illustrate median compositions of clasts from each seamount. The clasts differ in composition (most obviously with regard to K_2O and LOI) from Pacific Plate seamounts, implying metasomatic composition changes in the subduction zone. Data from this study, Fryer et al. (2018), and Deng et al. (2021). Compositions of Pacific seamounts are shown for comparison (see Section 2.1 for more information and data sources; $\tilde{x}$ = median compositions).

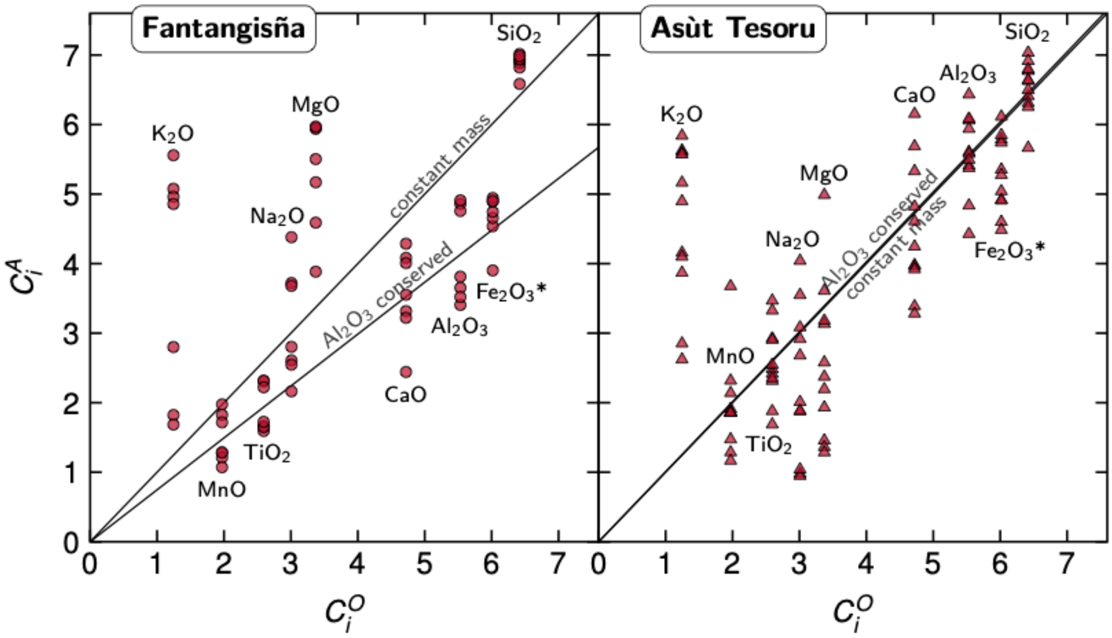

Figure 4: Isocon plots comparing the anhydrous compositions of the recycled OIBs (C_i^A) to the median of the NW Pacific seamounts (C_i^O). The net mass of samples from Fantangisña Seamount appears to have increased together with gains in K_2O, SiO_2, MgO, and Na_2O, whereas the net mass of the Asùt Tesoru Seamount samples did not significantly change and the clasts are merely enriched in K_2O and some in SiO_2. The lines shown for Al_2O_3-conservation are based on the mean Al_2O_3 contents; at Asùt Tesoru, the lines of constant mass and Al_2O_3-conservation are almost identical. The concentrations are scaled by the following divisors: SiO_2, 7.5; Al_2O_3, 3; Fe_2O_3*, 2; MnO, 0.1; MgO, 2; CaO, 2.

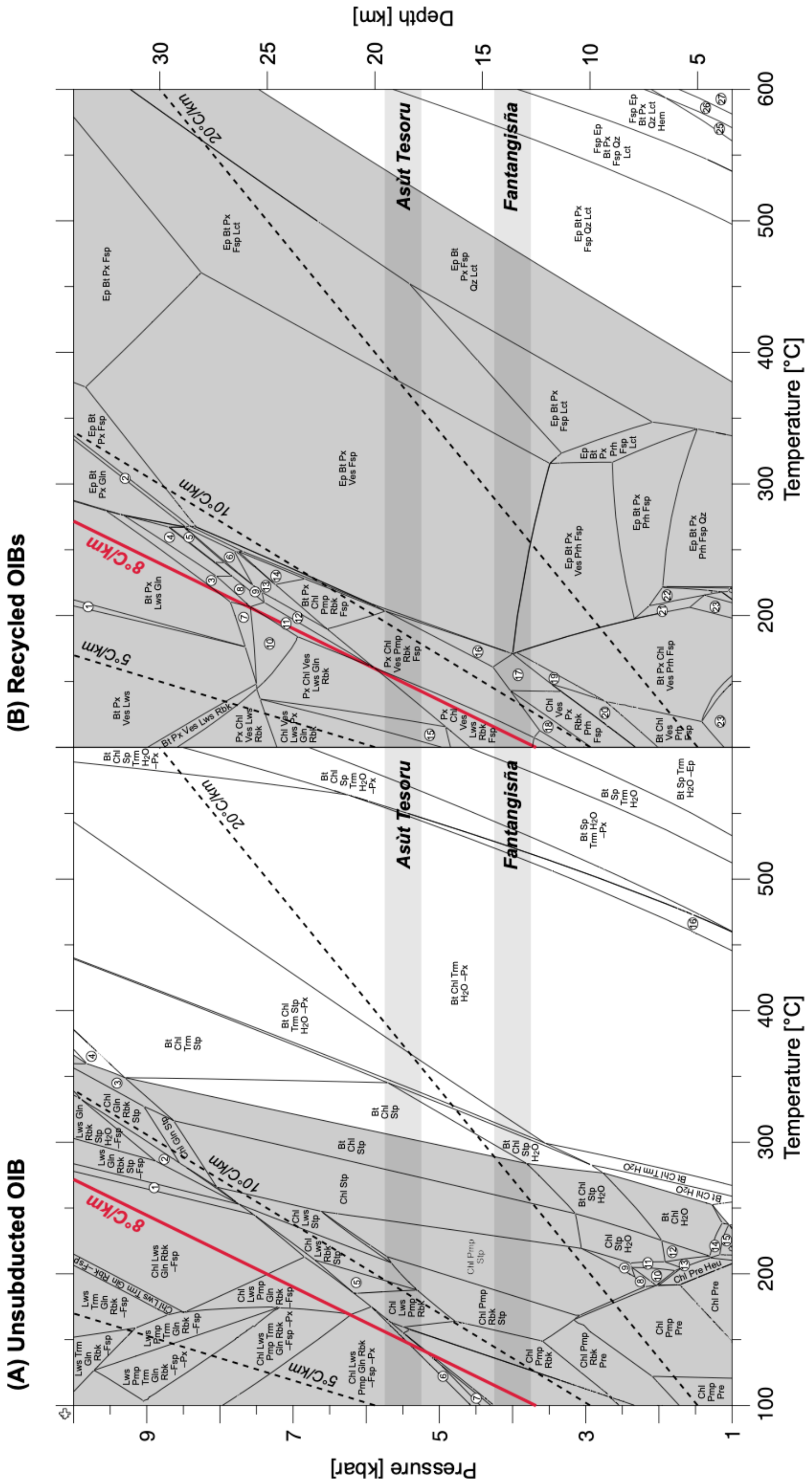

Figure 5: Equilibrium assemblage diagrams for **(A)** unsubducted OIB and **(B)** OIBs recycled by the serpentinite mud volcanoes. The predicted stability of phengite is indicated by the gray background. Note the considerably larger stability field of phengite in the metasomatized, recycled OIBs (B). Quantities of

metamorphic phases along the 8°C/km geotherm (red line) are shown in Fig. 6. Estimated *P* conditions at the top of the slab beneath Fantangisña and Asùt Tesoru Seamounts are indicated by gray bars. In (A): Qz, Fsp, Ep, and Px are present at all *P*/*T* conditions, unless indicated otherwise; 1, Chl Lws Gln Rbk Stp – Fsp; 2, Lws Gln Rbk Stp; 3, Bt Chl Gln Stp; 4, Bt Chl Gln Stp; 5, Chl Lws Rbk; 6, Chl Lws Pmp Gln Rbk –Px; 7, Chl Pmp Gln Rbk –Px; 8, Chl Pmp Stp Heu; 9, Chl Pmp Stp H_2O; 10, Chl Stp Heu; 11, Chl Stp Heu H_2O; 12, Chl H_2O; 13, Chl Heu H_2O; 14, Bt Chl Heu H_2O; 15, Bt Chl Heu; 16, Bt Chl Trm H_2O –Px. In (B): H_2O is present at all *P*/*T* conditions, unless indicated otherwise; 1, Bt Px Lws; 2, Ep Bt Px Gln Fsp; 3, Bt Px Lws Pmp Gln; 4, Px Lws Pmp Gln; 5, Px Pmp Gln Fsp; 6, Bt Px Pmp Gln Fsp; 7, Bt Px Ves Lws Gln; 8, Px Lws Pmp Gln Rbk; 9, Px Pmp Gln Rbk Fsp; 10, Bt Px Ves Lws Gln Rbk; 11, Px Ves Lws Pmp Gln Rbk; 12, Px Ves Pmp Gln Rbk Fsp; 13, Bt Px Pmp Gln Rbk Fsp; 14, Bt Px Chl Pmp Fsp; 15, Chl Ves Lws Px Gln Rbk; 16, Ep Px Chl Ves Rbk Fsp; 17, Px Chl Ves Rbk Prh Fsp; 18, Chl Ves Pmp Px Rbk Prh Fsp; 19, Bt Px Chl Ves Rbk Prh Fsp; 20, Bt Chl Ves Rbk Prh Fsp; 21, Ep Bt Px Chl Prh Fsp; 22, Ep Bt Px Prh Stp Fsp; 23, Bt Chl Ves Prh Fsp Stp; 24, Bt Px Chl Prh Fsp; 25, Fsp Bt Px Qz Lct Hem; 26, Fsp Bt Px Sp Qz Lct Hem; 27, Fsp Bt Px Sp Qz Lct. Abbreviations: Bt, biotite; Chl, chlorite; Ep, epidote; Fsp, feldspar; Gln, glaucophane; Hem, hematite; Heu, heulandite; Lct, leucite; Lws, lawsonite; Pmp, pumpellyite; Prh, prehnite; Px, pyroxene; Qz, quartz; Rbk, riebeckite; Sp, spinel; Stp, stilpnomelane; Trm, tremolite; Ves, vesuvianite.

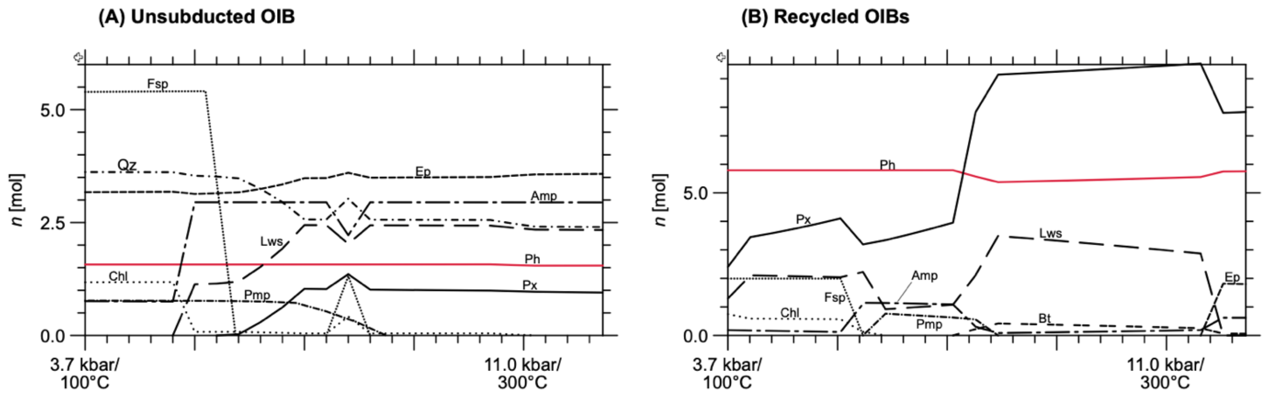

Figure 6: Mineral assemblages and quantities as predicted for **(A)** unsubducted OIB and **(B)** recycled OIBs along an 8°C/km geotherm. In addition to the much larger stability field of phengite (see Fig. 5b) it is also remarkably higher amounts of phengite that are predicted for the composition of the recycled OIBs. In (A), amphibole is tremolitic at low *P*/*T* and glaucophane–riebeckite above ~5–6 kbar/150°C, pyroxene is diopside to aegirine in composition (see also Fig. S3a). Amphibole in (B) is glaucophane to riebeckite, and pyroxene includes components of diopside, aegirine, and jadeite (Fig. S3b); biotite is phlogopitic. Phases with abundances <0.5 mol are not shown; these are the zeolite-group mineral stilbite (at 3.5 kbar/100°C) and vesuvianite (up to ~7 kbar/<200°C) in (B). Abbreviations: Amp, amphibole; Ph, phengite; others as in Fig. 5.

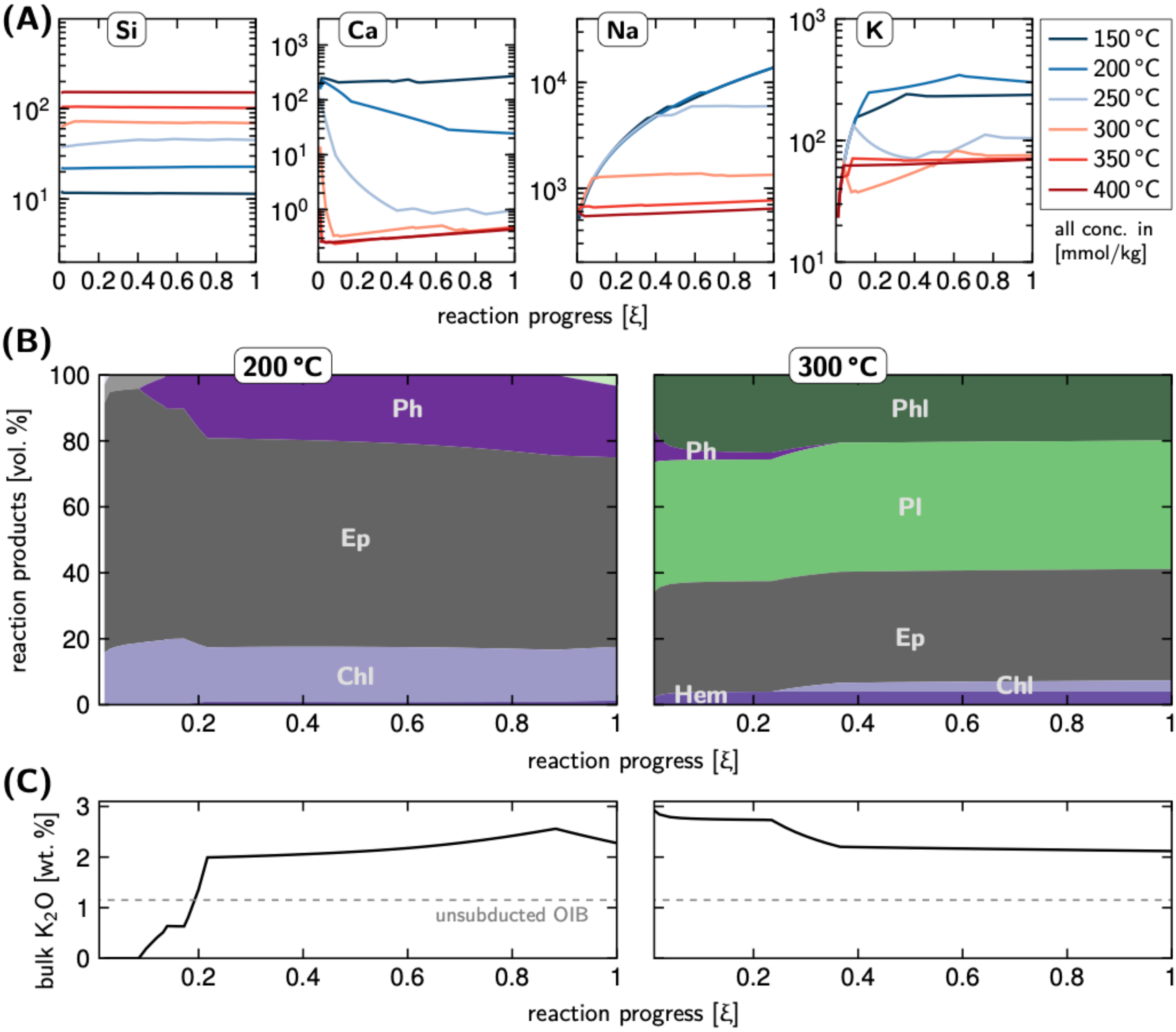

Figure 7: Results of reaction path models. The x-axes depict decreasing f/r ratios (with increasing reaction progress, ξ). **(A)** Modeled solute concentrations (mmol/kg) in a fluid after its equilibration with AOC (composition from Staudigel, 2014) at $P = 5$ kbar, varying T, and a f/r ratio of 0.1 at $\xi = 1$. Fluids equilibrated with AOC in a rock-dominated system, as is likely the case in subducting lithosphere, contain generally high K and Na; at $T < 200$°C, these solutes are particularly enriched. Calcium contents are also high at low T; those of Si increase with increasing T. Corresponding phase assemblages are shown in Figure S7. **(B)** Equilibrium phase assemblage predictions for OIB (median composition of NW Pacific seamounts; cf. Tab. 3) after the reaction with AOC-derived fluids shown in (A) at 200°C and 300°C, respectively, with a f/r ratio of 10 at $\xi = 1$. At 200°C, phengite is predicted at variably f/r ratios; at 300°C, phengite forms at high f/r ratios whereas the dominating K-bearing phase at lower f/r ratios is phlogopite. **(C)** Bulk rock K_2O contents that correspond to the phase assemblages in (B). At both T, K_2O of the metasomatized OIBs is markedly enriched relative to the starting composition (median NW Pacific

seamount with K_2O = 1.15 wt.%; dashed line). Abbreviations: Ph, phengite; Phl, phlogopite; Pl, plagioclase; others as in Fig. 5.

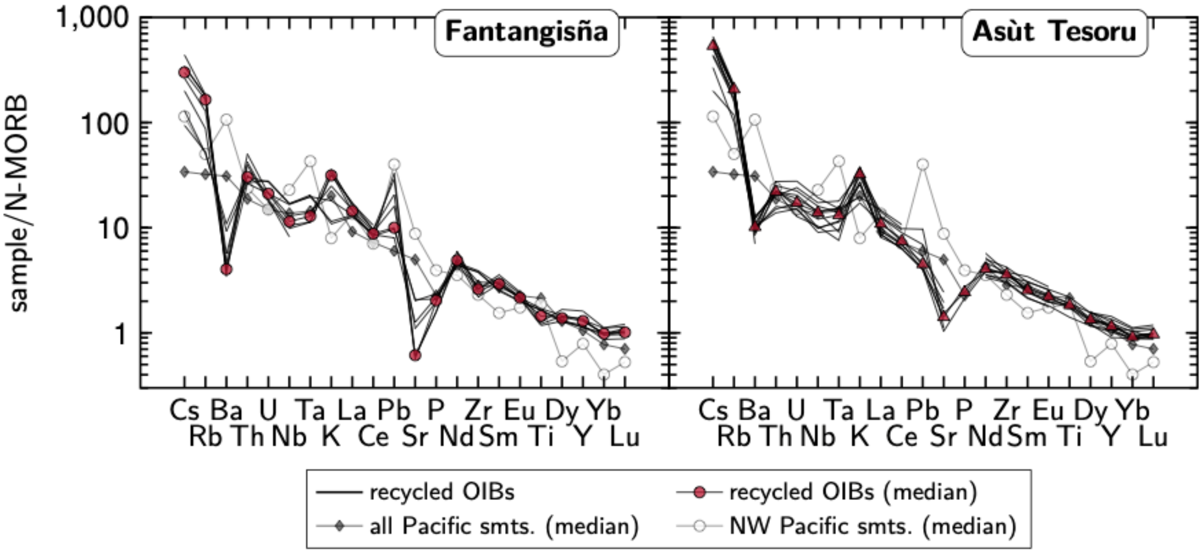

Figure 8: Multielement diagram for the recycled OIBs from Fantangisña and Asùt Tesoru Seamounts normalized to N-type mid-ocean ridge basalt (Sun & McDonough, 1989). Data for the recycled OIBs are from Fryer et al. (2018; 2020) and Deng et al. (2021), with K, P, and Ti values calculated from wt% oxide. Compositions of Pacific seamounts are shown for comparison (see Section 2.1 for more information and data sources; Ba values are only available for the Magellan Seamounts and are calculated from wt% oxide).

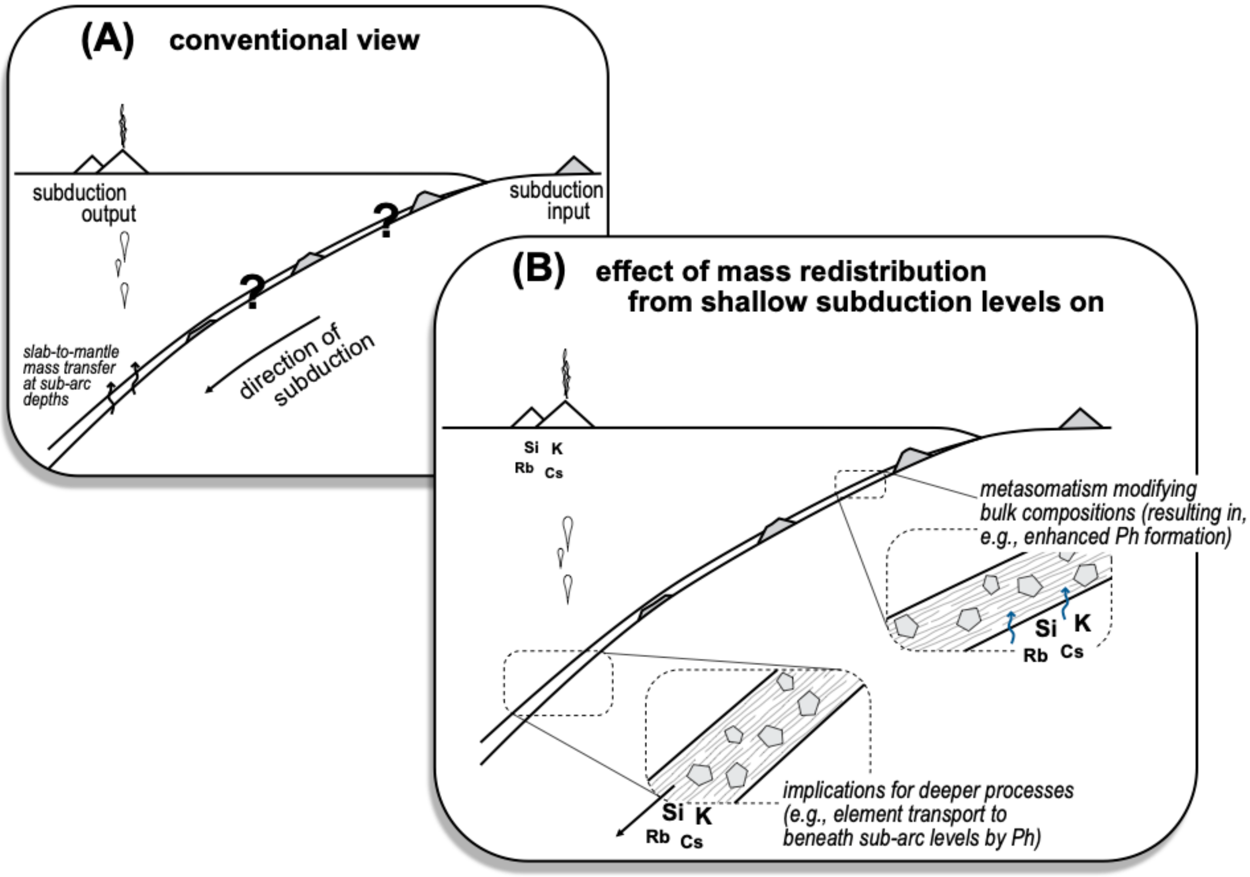

Figure 9: Interpretative conceptual sketch of metasomatism at shallow depths and its implications. **(A)** Conventional approach in which subduction inputs are compared with arc volcano outputs. This concept mostly takes account of subduction metamorphism affecting incoming lithologies, but metasomatism is in many cases ignored. **(B)** Mass transfer and metasomatism within the subduction system occur from very shallow levels on. These processes can produce entirely new bulk compositions with mineral assemblages that differ from those in the metamorphosed subducting lithologies of (A). Such shallow subduction processes can affect element redistribution and cycling at deeper levels. In this study we demonstrate that K and other solutes are mobilized in the Mariana subduction zone at $T \leq 200°C$; they are subsequently picked up in metavolcanics and incorporated in phengite, which likely transports them into the deep mantle.

Tables

Table 1: Summarized bulk rock compositional characteristics of the recycled OIBs. Data are from this study and from Fryer et al. (2018) and Deng et al. (2021); all data in wt%.

	SiO2	TiO2	Al2O3	Fe2O3*	MnO	MgO	CaO	Na2O	K2O	Sum	LOI
min	42.17	1.49	9.56	7.27	0.1	2.45	4.56	0.93	1.57	97.94	3.99
max	50.74	3.32	18.76	11.62	0.35	11.82	11.67	4.08	5.51	100.2	7.77
median	48.18	2.18	14.53	9.34	0.17	6.55	7.59	2.49	4.59	99.91	5.31
σ	2.04	0.54	2.73	1.12	0.06	3.11	1.77	0.93	1.28	0.64	0.92

Note: Fe2O3* = total FeO; LOI, loss on ignition.

σ = standard deviation = $\sqrt{(\,(\,\Sigma(\,x(i) - \mathrm{mean}(x)\,)\,\hat{}\,2\,)\,/\,n\,)}$

Table 2: Reference bulk rock compositions of Pacific seamounts (see Section 2.2). All data in wt%.

		SiO2	TiO2	Al2O3	Fe2O3*	MnO	MgO	CaO	Na2O	K2O	LOI	Ti	V	Ti/V
All data	median	47.88	2.79	14.69	11.75	0.17	6.15	10.00	2.90	0.89	2.12	16260	278	53.1
	σ	4.29	0.99	2.32	2.41	0.21	4.22	2.82	1.10	1.15	2.54	5457	95.5	434.3
	n	2382	2391	2382	2375	2357	2417	2380	2376	2441	731	241	1152	152
N hemisphere	median	48.30	2.62	14.10	11.90	0.17	6.47	9.98	2.66	0.64	2.02	14717	268	51.2
	σ	3.66	0.81	2.28	1.98	0.05	4.46	2.54	0.99	0.98	2.52	3936	85.0	33.6
	n	1291	1292	1289	1291	1291	1291	1289	1293	1326	433	143	600	128
NW Pacific	median	46.40	2.65	16.00	11.60	0.20	6.50	9.10	2.90	1.15	3.20	14320	255	72.0
	σ	3.58	0.73	1.47	2.35	0.07	2.74	2.73	0.76	1.69	1.72	2331	85.8	39.2
	n	91	84	86	74	86	86	86	86	86	74	7	85	7
MgO-filtered	median	47.49	2.38	13.00	11.64	0.17	9.96	10.11	2.36	0.49	1.03	12660	268	49.6
	σ	2.82	0.77	1.91	1.58	0.03	1.97	2.05	0.46	0.55	2.46	4890	47.9	10.3
	n	431	430	433	430	427	437	433	430	431	180	48	274	36
Ti/V-filtered	median	47.47	2.93	14.29	11.94	0.17	6.47	9.92	2.90	0.95	2.16	17831	282	61.3
	σ	2.07	0.63	1.84	1.38	0.05	3.51	2.08	0.95	0.69	3.71	3592	62.5	13.5
	n	75	75	75	75	75	75	75	75	75	55	75	75	75
MgO–Ti/V-filtered	median	47.10	2.39	13.20	11.94	0.17	10.00	9.97	2.40	0.42	3.14	15213	273	53.7
	σ	1.22	0.43	1.04	0.68	0.01	1.45	1.38	0.30	0.50	2.69	3576	30.8	9.6
	n	17	17	17	17	17	17	17	17	17	9	17	17	17

Note: Fe2O3* = total FeO; LOI = loss on ignition.

σ = standard deviation = √((Σ (x(i) - mean(x)) ^2) / n)

n = number of analyses

Table 3: Results of isocon analysis, relative to OIB from the NW Pacific (cf. Tab. 2), assuming the conservation of Al_2O_3. Calculations were done on an anhydrous basis.

Sample	Mud volcano	Reference	SiO2	TiO2	Al2O3	Fe2O3*	MnO	MgO	CaO	Na2O	K2O
U1497A-8F-2, 14–17 cm	Fantangisña	Deng et al. (2021)	1.17	1.01	1.00	0.86	1.14	1.75	1.03	1.41	1.67
U1497A-11G-CC, 22–25 cm	Fantangisña	Deng et al. (2021)	1.23	1.01	1.00	0.73	1.04	1.53	0.85	1.64	1.53
U1497A-12F-1, 78–81 cm	Fantangisña	Deng et al. (2021)	1.25	1.00	1.00	0.90	1.01	1.34	1.01	1.42	2.62
U1498B-23R-1, 60–63 cm	Fantangisña	Deng et al. (2021)	1.75	1.00	1.00	1.28	1.06	2.65	1.38	1.41	6.62
U1498B-23R-1, 67 cm	Fantangisña	this study	1.61	0.97	1.00	1.23	0.93	2.68	1.06	1.41	6.03
U1498B-23R-1, 67–69 cm	Fantangisña	Deng et al. (2021)	1.70	1.00	1.00	1.29	1.02	2.77	1.07	1.33	6.13
U1498B-23R-1, 70–75 cm	Fantangisña	Deng et al. (2021)	1.58	0.96	1.00	1.18	0.79	2.57	0.75	1.04	6.48
U1496B-8X-CC, 0–2 cm	Asùt Tesoru	Deng et al. (2021)	1.32	1.20	1.00	1.27	0.93	0.81	1.12	1.68	4.17
U1496B-8X-CC, 0–4 cm	Asùt Tesoru	Fryer et al. (2018)	1.02	1.00	1.00	0.98	0.96	0.44	1.33	1.21	2.15
U1496B-8X-CC, 8–13 cm	Asùt Tesoru	Fryer et al. (2018)	1.02	0.92	1.00	0.94	0.96	0.40	1.01	0.96	3.25
U1496B-8X-CC, 30–32 cm	Asùt Tesoru	Fryer et al. (2018)	1.13	0.92	1.00	0.84	0.67	0.39	0.87	0.92	4.65
U1496B-8X-CC, 33–41 cm	Asùt Tesoru	Deng et al. (2021)	1.23	1.04	1.00	1.02	0.68	0.81	0.82	1.17	5.37
U1496B-10F-2, 0–5 cm	Asùt Tesoru	Fryer et al. (2018)	1.05	1.33	1.00	0.87	1.85	0.57	0.69	0.62	4.46
U1496B-10F-2, 5–8 cm	Asùt Tesoru	Fryer et al. (2018)	1.04	0.73	1.00	0.77	1.09	0.77	1.21	0.67	3.13
U1496B-10F-2, 13 cm	Asùt Tesoru	this study	0.85	0.56	1.00	0.64	0.81	0.80	0.84	0.54	3.57
U1496B-10F-2, 14 cm	Asùt Tesoru	this study	0.89	1.02	1.00	0.76	0.85	0.97	0.75	0.31	4.07
U1496B-10F-2, 17–20 cm	Asùt Tesoru	Fryer et al. (2018)	0.92	1.03	1.00	0.74	0.87	0.86	0.77	0.30	3.59
U1496B-10F-2, 35 cm	Asùt Tesoru	this study	0.82	1.19	1.00	0.91	1.10	1.38	1.05	0.29	2.13

Note: Fe2O3* = total FeO; LOI, loss on ignition.